JCI The Journal of Clinical Investigation

Zeb1 modulates hematopoietic stem cell fates required for suppressing acute myeloid leukemia

Alhomidi Almotiri, … , Florian A. Siebzehnrubl, Neil P. Rodrigues

J Clin Invest. 2020. https://doi.org/10.1172/JCI129115.

Research In-Press Preview Hematology Stem cells

Graphical abstract

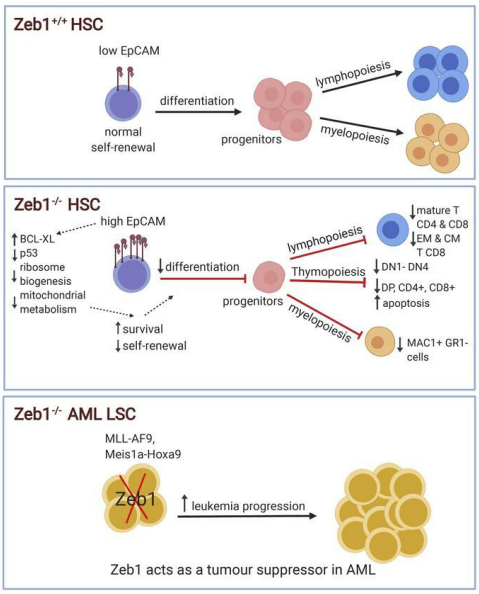

Zeb1 modulates hematopoietic stem cell fates required for suppressing acute myeloid leukemia

Alhomidi Almotiri[1,2], Hamed Alzahrani[1], Juan Bautista Menendez-Gonzalez[1], Ali Abdelfattah[1], Badi Alotaibi[1], Lubaid Saleh[1], Adelle Greene[1], Mia Georgiou[1], Alex Gibbs[1], Amani Alsayari[1], Sarab Taha[1], Leigh-Anne Thomas[1], Dhruv Shah[1], Sarah Edkins[3], Peter Giles[3], Marc P. Stemmler[4], Simone Brabletz[4], Thomas Brabletz[4], Ashleigh S. Boyd[5,6#], Florian Siebzehnrubl[1#] and Neil P. Rodrigues[1#*]

[1]European Cancer Stem Cell Research Institute, Cardiff University, School of Biosciences, Cardiff, UK

[2]Faculty of Applied Medical Sciences, Shaqra University, AlDuwadimi, Saudi Arabia

[3]Wales Gene Park and Wales Cancer Research Centre, Division of Cancer and Genetics, Cardiff University, School of Medicine, Cardiff, UK

[4]Department of Experimental Medicine 1, Nikolaus-Fiebiger-Center for Molecular Medicine, FAU University Erlangen-Nürnberg, Erlangen, Germany.

[5]Department of Surgical Biotechnology, Division of Surgery and Interventional Science, Royal Free Hospital, University College London, London, UK

[6]Institute of Immunity and Transplantation, University College London, London, UK

[#] Co-senior authors

*****Corresponding author:
Neil P. Rodrigues
email: rodriguesn@cardiff.ac.uk

Abstract

Zeb1, a zinc finger E-box binding homeobox epithelial-mesenchymal (EMT) transcription factor, confers properties of 'stemness', such as self-renewal, in cancer. Yet little is known about the function of *Zeb1* in adult stem cells. Here, we used the hematopoietic system, as a well-established paradigm of stem cell biology, to evaluate *Zeb1* mediated regulation of adult stem cells. We employed a conditional genetic approach using the *Mx1-Cre* system to specifically knockout (KO) *Zeb1* in adult hematopoietic stem cells (HSCs) and their downstream progeny. Acute genetic deletion of *Zeb1* led to rapid onset thymic atrophy and apoptosis driven loss of thymocytes and T cells. A profound cell-autonomous self-renewal defect and multi-lineage differentiation block was observed in *Zeb1* KO HSCs. Loss of *Zeb1* in HSCs activated transcriptional programs of deregulated HSC maintenance and multi-lineage differentiation genes, and of cell polarity, consisting of cytoskeleton, lipid metabolism/lipid membrane and cell adhesion related genes. Notably, Epithelial cell adhesion molecule (EpCAM) expression was prodigiously upregulated in *Zeb1* KO HSCs, which correlated with enhanced cell survival, diminished mitochondrial metabolism, ribosome biogenesis, and differentiation capacity and an activated transcriptomic signature associated with acute myeloid leukemia (AML) signaling. *ZEB1* expression was downregulated in AML patients and *Zeb1* KO in the malignant counterparts of HSCs - leukemic stem cells (LSCs) - accelerated *MLL-AF9* and *Meis1a/Hoxa9*-driven AML progression, implicating *Zeb1* as a tumor suppressor in AML LSCs. Thus, *Zeb1* acts as a transcriptional regulator in hematopoiesis, critically co-ordinating HSC self-renewal, apoptotic and multi-lineage differentiation fates required to suppress leukemic potential in AML.

Introduction

Epithelial-mesenchymal transition (EMT) is a complex process that organizes specific changes in cellular fate and phenotype and is usually accompanied by loss of cell polarity and adhesion and increased locomotion (1). EMT is an important step in embryonic development and regeneration, which largely promotes a program of cellular plasticity and migration (2). This program is regulated by specific transcription factors (TFs), such as members of the ZEB, SNAI, and TWIST families. To this end, *Zeb1*, a zinc finger TF that binds to E-box motifs, has been implicated in myogenesis (3-6), neuronal development and differentiation (7-10), post gastrulation embryogenesis (11) and T-cell development (12, 13).

It has also been posited that EMT is a critical regulator in cancer pathogenesis and, in particular, cancer stem cell behavior (14-16), which facilitates cancer cells becoming more metastatic with resultant tumor progression (17). Abundant evidence shows that *Zeb1* regulates stem cell properties in cancer including self-renewal (18-20). While it is established that *Zeb1* regulates expression of multiple stem cell-associated transcription factors, including those with oncogenic potential, such as BMI1, KLF4, and SOX2 (19, 21), and that loss of *Zeb1* promotes cellular differentiation during development of the embryonic CNS (9), and skeletal muscle (22), the wider role of *Zeb1* in normal stem cell fate decisions remains unclear.

By exploiting a mouse model engineered to contain conditional alleles of *Zeb1* and an inducible *Mx-1-Cre* (*Zeb1*$^{fl/fl}$*;Mx1-Cre*$^{+}$) (23), where *Zeb1* expression can be deleted in hematopoietic stem cells (HSCs) and their progeny by administering polyinosinic-polycytidylic acid (pIpC), we used the hematopoietic system, as an established stem cell model, to evaluate *Zeb1* mediated regulation of somatic stem cells. Herein, we identify *Zeb1* as a crucial, indispensable regulator of adult T cell maturation and differentiation. In a broader context, as judged by conditional deletion within the hematopoietic system, we identify *Zeb1* as an essential transcriptional repressor balancing adult stem cell self-renewal, apoptotic and global, multi-lineage differentiation fates of stem cells. Finally, we find that *Zeb1* mediated regulation of these stem cell fates is required to suppress malignancy in the context of acute myeloid leukemia (AML).

Results

Acute conditional deletion of *Zeb1* reduces the frequency of MAC1$^+$ myeloid cells and CD8$^+$ memory T cells

Zeb1 expression has been observed in hematopoietic cells from bone marrow (BM), thymus, spleen, fetal liver and lymph nodes (12, 24). However, *Zeb1* expression pattern in different subsets of hematopoietic cells, including hematopoietic stem and progenitor cells (HSPCs), remains unclear. We therefore conducted Q-PCR analysis of *Zeb1* expression in hematopoietic cell compartments prospectively isolated by fluorescent-activated cell sorting (FACS). *Zeb1* was expressed at high levels in stem and progenitor cells (HSC, MPP (Multipotent progenitor), HPC1 (hematopoietic progenitor cell 1), and HPC2 (hematopoietic progenitor cell 2)) and in terminally differentiated cells (myeloid, erythroid, B, and T lineages) whereas it was lower in committed myeloid and lymphoid progenitors (CMP (common myeloid progenitors), GMP (granulocyte-monocyte progenitors), MEP (megakaryocyte-erythroid progenitors), CLP (common lymphoid progenitors)) (**Figure 1A**).

To evaluate the genetic requirement for *Zeb1* in adult HSCs, their progenitors and fully differentiated blood and immune cells, we bred mice harboring conditional alleles of *Zeb1* (*Zeb1*$^{fl/fl}$ mice) (23) with *Mx1-Cre* (25) to obtain either *Zeb1*$^{fl/fl}$*;Mx1-Cre*$^{+/-}$ or control (*Zeb1*$^{fl/fl}$*;Mx1-Cre*$^{-/-}$) mice and administered pIpC on alternate days for 10 days to achieve deletion of *Zeb1* (*Zeb1*$^{-/-}$). Hematopoiesis in control or *Zeb1*$^{-/-}$ mice was analyzed 14 days after the last dose of pIpC (**Figure 1B**). *Zeb1* was partially deleted in total BM cells (**Figure 1C**). To assess whether *Zeb1* was completely deleted in HSCs from BM, we

prospectively isolated Lin^- $SCA\text{-}1^+$ $C\text{-}KIT^+$ (LSK) cells (that contain HSCs) and, by genomic PCR, observed complete deletion of *Zeb1* (**Figure 1C**). Similarly, $C\text{-}KIT^+$ cells, which constitute both HSCs and committed myeloid and lymphoid progenitors, were fully deleted for *Zeb1* (**Figure 1D**). In contrast, only partial deletion of *Zeb1* was observed in terminally differentiated T and B cells isolated from the spleen (**Figure 1D**), suggesting that incomplete deletion observed in BM cells may be ascribed to these cell types.

At 14 days after ablation of *Zeb1*, no significant changes were observed in BM and spleen cellularity or spleen size (**Supplemental Figure 1A**). Immunophenotyping of peripheral blood (PB) revealed a significant reduction in the proportion of $MAC1^+$ $GR1^-$ monocytic cells in *Zeb1*$^{-/-}$ mice, while no significant changes were observed in $MAC1^+$ $GR1^+$ cells, that contain granulocytes, or in T cells and B cells in PB or BM (**Figure 1E and Supplemental Figure 1B**) (26, 27). Intriguingly, despite incomplete deletion of *Zeb1* in lymphoid cells from *Zeb1*$^{-/-}$ mice, we observed a selective reduction in $CD8^+$ effector memory ($CD8^+$ EM) ($CD44^{high}$ $CD62L^-$) T cells in PB and BM of *Zeb1*$^{-/-}$ mice (**Figure 1, F and G**). We also found a reduction in $CD8^+$ central memory ($CD8^+$ CM) ($CD44^{high}$ $CD62L^{high}$) T cells in spleen of *Zeb1*$^{-/-}$ mice, collectively demonstrating a critical role of *Zeb1* in $CD8^+$ T cell function (**Figure 1H**).

Acute loss of *Zeb1* results in a cell survival defect during thymocyte differentiation and a cell-autonomous T cell differentiation defect

Having shown a defect in $CD8^+$ T cells in *Zeb1*$^{-/-}$ mice and given that germ-line KO of *Zeb1* results in a developmental defect in the T cell lineage (12, 13), we opted to assess T cell development in the thymus of adult *Zeb1*$^{-/-}$ mice. Fourteen days after the last dose of pIpC, *Zeb1*$^{-/-}$ mice displayed diminutive thymi coupled with a dramatic reduction in cellularity (**Figure 2, A-C**). Immunophenotypic analysis of T cell subsets in the thymus revealed an increased frequency of immature double negative $CD4^-$ $CD8^-$ (DN) cells and mature single positive (SP) CD4 ($CD4^+$) and SP CD8 ($CD8^+$) T cells contrasting with a significant reduction in the proportion of double positive $CD4^+$ $CD8^+$ (DP) cells in *Zeb1*$^{-/-}$ mice (**Figure 2, D and E**). Normalizing for reduced thymic cellularity in *Zeb1*$^{-/-}$ mice led to a significant reduction in total cell numbers observed in DN, DP, $CD4^+$ and $CD8^+$ cells from *Zeb1*$^{-/-}$ mice (**Figure 2F**). This correlates with increased apoptosis in DP, $CD4^+$ and $CD8^+$ populations but, surprisingly, not in DN cells from *Zeb1*$^{-/-}$ mice (**Supplemental Figure 1C**).

Given that the earliest stages of T cell development were affected by *Zeb1* ablation, we further evaluated the DN cell compartment, which represents the initial stage of thymocyte selection (28, 29). Using CD44 and CD25, the DN population can be subdivided chronologically into 4 populations: DN1 ($CD44^+$ $CD25^-$), DN2 ($CD44^+$ $CD25^+$), DN3 ($CD44^-$ $CD25^+$), and DN4 ($CD44^-$ $CD25^-$) (29) before they become DP cells and ultimately $CD4^+$ or $CD8^+$ mature cells (29). Immunophenotypic analysis showed increased frequency of DN1 cells and a reduction in DN2 and DN3 while no change was observed in the frequency of DN4 in *Zeb1*$^{-/-}$ mice, suggestive of a *Zeb1* mediated differentiation block in the transition between DN1 and DN2/DN3 (**Figure 2, G-H**). Analysis of

apoptosis in DN subsets revealed increased apoptotic levels in DN2 and DN3 after *Zeb1* deletion, accounting for the differentiation block observed in these compartments, whereas DN1 and DN4 displayed comparable levels of apoptosis between genotypes (**Supplemental Figure 1D**). When the absolute number of these populations was quantified to account for reduced thymic cellularity of *Zeb1*$^{-/-}$ mice, a significant decrease was found across all DN populations following *Zeb1* deletion (**Figure 2I**).

Next, we evaluated whether the defect observed within immature DN cells was caused by a failure of thymocyte survival preceding selection. We therefore assessed early thymic progenitors (ETPs), characterized as CD4^{-} CD8^{-} CD44^{+} CD25^{-} C-KIT^{high} (30-33). Fourteen days after the last dose of pIpC, we found a comparable frequency of ETPs between control and *Zeb1*$^{-/-}$ mice (**Figure 2J**) with the absolute count of ETPs in *Zeb1*$^{-/-}$ thymus showing a near significant reduction compared to control due to reduced thymic cellularity in *Zeb1*$^{-/-}$ mice (**Figure 2K**).

Since the *Mx1-Cre* system deletes genes in non-hematopoietic tissues, such as BM niche cells (25, 34), we assessed whether *Zeb1* mediated regulation of T cell development was cell-autonomous by competitively transplanting CD45.2^{+} BM cells from *Zeb1*$^{fl/fl}$*;Mx1-Cre*$^{+}$ or control mice, admixed with unfractionated CD45.1^{+} BM cells (**Supplemental Figure 2A**). Six weeks post-transplantation *Zeb1* deletion was induced by injection of pIpC and 14 days after the last pIpC injection analysis of donor engraftment in the thymus revealed a dramatic reduction in the *Zeb1*$^{-/-}$ genotype compared to control

(**Supplemental Figure 2B**). Consistent with this, a substantial attenuation in donor contribution to DN, DP, $CD4^+$, and $CD8^+$ cell population were detected in the *Zeb1*$^{-/-}$ genotype (**Supplemental Figure 2C**). With the exception of ETPs, a significant reduction in donor contribution was found across nearly all DN populations following cell-autonomous *Zeb1* deletion, confirming that *Zeb1* mediates T cell maturation in a cell-autonomous manner (**Supplemental Figure 2D**). Since mature T cell frequency did not change 14 days after *Zeb1* loss during steady state due to incomplete *Zeb1* deletion **(Figure 1D)**, we also analyzed the donor contribution to peripheral T cells 14 days after *Zeb1* ablation in a cell-autonomous manner, which revealed complete deletion of *Zeb1* and a significant reduction in mature T cells in PB, BM, and spleen **(Supplemental Figure 2, E and F)**. Further, we confirmed that *Zeb1* mediates cell-autonomous reduction in EM $CD8^+$ T cells in PB (**Supplemental Figure 2G**). Together, these data suggest that *Zeb1* is critical for cell survival at the earliest stages of thymocyte differentiation as well as for T cell maturation and maintenance in the thymus. Thus, *Zeb1* is required for cell-autonomous T cell development in the thymus.

Acute conditional deletion of *Zeb1* results in a reduction of lymphoid lineage commitment in BM

We next gauged the impact of *Zeb1* on early T-lymphoid lineage commitment in the BM. LSK $CD135^{high}$ $CD127^{high}$ lympho-myeloid multipotent progenitors (LMPPs $CD127^+$, non-conventional LMPP) rapidly and efficiently generate T and innate lymphoid cells (35) compared with conventional LMPP (LSK $CD34^+$ $CD135^{high}$) (36) or HPC1 (LSK $CD150^-$ $CD48^+$) that overlap functionally with

conventional LMPP by 80% (37-39). Interestingly, we found a significant reduction in the proportion of T-cell lineage primed LMPP $CD127^{+}$ but not conventional LMPP, which showed a statistically insignificant trend towards reduction after acute *Zeb1* ablation (**Figure 3, A and B and Supplemental Figure 3A**). We assessed other BM lymphoid progenitor compartments, including CLP (LIN^{-} $SCA\text{-}1^{low}$ $C\text{-}KIT^{low}$ $CD127^{high}$ $CD135^{high}$) (35, 40) and LIN^{-} $SCA\text{-}1^{+}$ $C\text{-}KIT^{-}$ (LSK^{-}) $CD135^{+}$ $CD127^{+}$) (41) that were reduced in *Zeb1*$^{-/-}$ mice (**Figure 3, A and B**). Together, these data suggest that *Zeb1* acts as a critical modulator of incipient lymphoid progenitor commitment from HSCs.

Acute conditional deletion of *Zeb1* in HSCs results in a profound self-renewal and multi-lineage hematopoietic differentiation defect

To directly assess the impact of acute deletion of *Zeb1* in HSCs, we performed flow cytometry analysis on immunophenotypically defined HSCs and all multipotent progenitor populations from control or *Zeb1*$^{-/-}$ mice. The frequency of HSCs (LSK $CD150^{+}$ $CD48^{-}$) and MPPs (LSK $CD150^{-}$ $CD48^{-}$) was comparable between control and *Zeb1*$^{-/-}$ genotypes **(Supplemental Figure 3B)**. HPC1 (LSK $CD150^{-}$ $CD48^{+}$) showed a non-significant reduction after *Zeb1* deletion similar to that observed in conventional LMPP (LSK $CD34^{+}$ $CD135^{+}$) **(Supplemental Figure 3, A and B).** *Zeb1*$^{-/-}$ HPC2 (LSK $CD150^{+}$ $CD48^{+}$), which possesses both myeloid and lymphoid potential (38), showed a significant reduction in the frequency in total BM compared to control **(Supplemental Figure 3B).** These data demonstrate that *Zeb1* regulates the abundance of select multipotent progenitor populations.

Having observed a reduction of MAC1^{+} GR1^{-} myeloid cells in PB following acute deletion of *Zeb1* in the hematopoietic system, we asked whether this was due to defects in committed myeloid progenitors from BM *Zeb1*$^{-/-}$. No significant difference in CMP (LK CD34^{+} CD16/32^{-}), GMP (LK CD34^{+} CD16/32^{+}) and MEP (LK CD34^{-} CD16/32^{-}) populations was noted between control and *Zeb1*$^{-/-}$ mice (**Supplemental Figure 3C**). Thus, *Zeb1* mediated regulation of terminal MAC1^{+} GR1^{-} myeloid cell differentiation appears to be independent of committed myeloid progenitor maturation from BM.

To stringently test the functionality and differentiation capacity of HSCs from *Zeb1*$^{-/-}$ mice, we prospectively isolated 150 HSCs (CD45.2) from control or *Zeb1*$^{-/-}$ mice at 14 days following deletion, mixed them with 2x10^{5} BM competitor cells (CD45.1) and transplanted this cell preparation into lethally irradiated recipients (CD45.1) (**Figure 3C**). The engraftment capacity of transplant recipients in PB was monitored until week 16 (**Figure 3C**). Significant engraftment failure was observed by week 6 and continued to decrease progressively until week 16 (**Figure 3D**). To test the donor contribution to PB of specific hematopoietic lineages, we analyzed PB for CD45.2 (donor) and CD45.1 (competitor) in conjunction with MAC1^{+} GR1^{-} myeloid, MAC1^{+} GR1^{+} myeloid, B220^{+} B cells, and CD4^{+}/CD8^{+} T cells. A profound reduction in donor contribution to B cells (**Figure 3E**), MAC1^{+} GR1^{-} myeloid cells (**Figure 3F**), and MAC1^{+} GR1^{+} myeloid cells (**Figure 3G**) was observed in recipients of *Zeb1*$^{-/-}$ HSCs. No engrafted T cells were derived from recipients transplanted with *Zeb1*$^{-/-}$ HSCs (**Figure 3H**).

Having observed multi-lineage defects in terminally differentiated blood cells in recipients of *Zeb1*$^{-/-}$ HSCs, we asked whether these defects originated in parental HSPCs or lineage-committed progenitors. Within LSK compartments, the donor contribution to HSC was equal between recipients of control or *Zeb1*$^{-/-}$ HSCs (**Figure 3I**). However, there was a significant reduction in the donor contribution to MPP, HPC1, and HPC2 in *Zeb1*$^{-/-}$ compared to control (**Figure 3I**). We also analyzed committed progenitors downstream of HSPCs and found a dramatic reduction in donor contribution to CMP, GMP, MEP, and LSK^{-} CD127^{+} but no change was observed in donor contribution to CLP (**Figure 3J**). These data directly link the functional defects observed after transplantation of *Zeb1* deficient HSCs to alterations in specific HSPC and lineage committed progenitor compartments.

An integral part of successful engraftment after BM transplantation is homing of intravenously infused HSPCs to the BM niche, the main home of adult hematopoiesis. To assess whether the *Zeb1*$^{-/-}$ engraftment defect was due to abnormal homing of *Zeb1*$^{-/-}$ HSPCs to the BM, we transplanted 7x10^{6} total BM cells (CD45.2) from control or *Zeb1*$^{-/-}$ mice into lethally irradiated recipients (CD45.1) and analyzed donor cell presence in recipients at 18 hours after transplantation (**Supplemental Figure 4A**). Relative parity was observed in the homing capacity of total BM cells or LSK populations in the two genotypes (**Supplemental Figure 4B**). Similarly, homing of donor cells to the spleen and thymus was comparable between control and *Zeb1*$^{-/-}$ genotypes (**Supplemental Figure 4C**). Thus, acute deletion of *Zeb1* does not impact the homing ability of hematopoietic cells *in vivo*.

To directly test the impact of *Zeb1* deletion on the self-renewal capacity of HSCs we performed secondary transplantation of *Zeb1*$^{-/-}$ HSCs. We sorted 300 HSCs (CD45.2) from control or *Zeb1*$^{-/-}$ primary recipients and admixed them with 3x10^5 competitor BM cells before transplanting them into lethally irradiated recipients. We observed a strong defect in PB engraftment associated with multilineage hematopoietic impairment in secondary transplant recipients by week 12 (**Figure 4, A and B**), indicative of a self-renewal defect in *Zeb1*$^{-/-}$ HSCs.

Zeb1 is required for cell-autonomous HSC function

To assess whether the acute requirement for *Zeb1* in maintaining HSC function was cell-autonomous, we performed a competitive BM transplantation by transplanting 5x10^5 BM cells from control and *Zeb1*$^{fl/fl}$ *Mx1-Cre*$^+$ (CD45.2) mice admixed with equal number of WT competitor cells (CD45.1) into lethally irradiated recipients (CD45.1). Six weeks later, *Zeb1* deletion was induced by administering recipients with pIpC and 14 days after the last dose of pIpC, mice were sacrificed and 5x10^5 donor BM cells **(**CD45.2) from primary recipients (14 days after *Zeb1* ablation) mixed with 5x10^5 competitor BM cells (CD45.1) were transplanted into lethally irradiated recipients (**Figure 4C**). Sixteen weeks after transplantation, we found a dramatic reduction in donor engraftment in PB and BM (**Figure 4D**). Further analysis of donor contribution to PB lineages revealed a marked reduction in myeloid cells, and near loss of B and T cells (**Figure 4E**).

To test whether the *Zeb1*$^{-/-}$ BM microenvironment plays a role in *Zeb1*-mediated HSC regulation, we transplanted 1x10^6 wild type (WT) BM cells (CD45.1) into lethally irradiated control or *Zeb1*$^{fl/fl}$ *Mx1-Cre*$^+$ (CD45.2) mice. Six weeks later, we injected the recipients with pIpC to delete *Zeb1* and analyzed the mice at week 16 after the last dose of pIpC (**Supplemental Figure 4D**). PB analyses of myeloid cells (MAC1$^+$), B cells (B220$^+$), and T cells (CD4$^+$/CD8$^+$) showed no significant difference between control and *Zeb1*$^{-/-}$ (**Supplemental Figure 4E**). Next, we asked whether the altered BM niche would impact the composition of HSPC and committed progenitors. The data showed that the frequency of these populations was comparable between control and *Zeb1*$^{-/-}$ (**Supplemental Figure 4, F and G**). Together these data demonstrate that *Zeb1* is required for cell-autonomous HSC functionality.

Zeb1$^{-/-}$ HSCs display deregulated cell polarity and hematopoietic differentiation transcriptional signatures

In order to understand the transcriptional signature underpinning *Zeb1* mediated regulation in HSCs, we performed RNA sequencing on purified HSCs (LSK CD150$^+$ CD48$^-$) from control or *Zeb1*$^{-/-}$ mice 14 days after the last dose of pIpC. From 222 differentially expressed genes (DEG), 47 genes (21%) were downregulated and 175 upregulated (79%) from *Zeb1*$^{-/-}$ HSCs. These data are largely consistent with the notion that *Zeb1* functions as a transcriptional repressor (42). Biological pathway analysis confirmed that the most enriched pathways were upregulated and included tight junction, cell adhesion, cell junction organization, immune system and endocytosis pathways (**Figure 5A**). *Zeb1* appears to regulate a transcriptional signature related to cell polarity,

consisting of genes related to cytoskeleton, cell adhesion and lipid metabolism/lipid membrane biology **(Figure 5B)**, congruent with the idea that *Zeb1* acts as a potent inducer of the EMT process, involving *Zeb1*-mediated repression of cell polarity genes (43-45). Using Ingenuity Pathway Analysis, we generated a gene interaction network showing the direct regulation of *Zeb1*-specific target genes related to cell polarity, cytoskeleton, and cell adhesion that included a regulatory node involving Epithelial cell adhesion molecule (EpCAM), CRB3, PARD6b, ITGB4, CDH1, KRT18 and OCLN (10, 43-50) (**Figure 5C**). In agreement with this transcriptional network, EpCAM, CDH1 and ITGB4 upregulation in *Zeb1*$^{-/-}$ HSPCs was confirmed at the protein level by flow cytometry (**Figure 6, A and B and Supplemental Figure 5, A and B**). Reflecting the global, multi-lineage differentiation functional defects of *Zeb1*$^{-/-}$ HSCs, we observed a broad, robust pattern of deregulated HSC maintenance and hematopoietic lineage-affiliated from both myeloid and lymphoid lineages (**Figure 5B**).

With prominent transcriptional deregulation of T-cell pathways being observed in *Zeb1*$^{-/-}$ HSCs (**Figure 5A**), we next asked whether the defects in *Zeb1*$^{-/-}$ HSCs could be associated to those observed in *Zeb1*$^{-/-}$ T cells. To address this question at the transcriptional level, we conducted RNA sequencing from *Zeb1*$^{-/-}$ or control CLPs, which have T-lymphoid but not myeloid potential, and compared their transcriptional signature with that from *Zeb1*$^{-/-}$ HSCs. *Zeb1*$^{-/-}$ CLPs displayed comparable gene expression pathways to *Zeb1*$^{-/-}$ HSCs, including deregulated cell-cell junction, tight junction, cell adhesion, cytoskeleton and T cell pathways (**Supplemental Figure 5, C- E**). Remarkably,

of the 47 differentially expressed genes in *Zeb1*$^{-/-}$ CLPs, 27 genes (57%) were also differentially expressed in *Zeb1*$^{-/-}$ HSCs (**Supplemental Figure 5F**). Other biological pathways reflecting T-cell function were deregulated in *Zeb1*$^{-/-}$ HSCs but not *Zeb1*$^{-/-}$ CLPs (e.g. calcium-induced T lymphocyte apoptosis, iCOS-iCOSL signaling in T helper cells) (**Figure 5A**). Transcriptional signatures relating to the CtBP1 pathway (51, 52) were observed only in *Zeb1*$^{-/-}$ CLPs (**Supplementary Figure 5C**). However, the majority of transcriptional programing mediating the differentiation defect of *Zeb1*$^{-/-}$ T cells was instigated in HSCs and transmitted to CLPs. Overall, in its capacity as a transcriptional repressor, *Zeb1* acts as a potent regulator of cell polarity and differentiation-affiliated transcriptional signatures in HSCs.

Increased EpCAM expression confers a cell survival advantage in *Zeb1*$^{-/-}$ HSCs that alters self-renewal and differentiation fates.

EpCAM, a glycoprotein mediating cell adhesion in epithelia (53), was the most highly upregulated gene in *Zeb1*$^{-/-}$ HSCs (**Figure 5B**). In other types of stem cell, EpCAM has been established as a crucial regulator of stem cell maintenance and differentiation (46). We therefore elected to examine the impact of EpCAM expression in the context of *Zeb1* mediated regulation of HSC fate. We first confirmed enhanced expression of EpCAM at the protein level by flow cytometry of *Zeb1*$^{-/-}$HSCs, MPP, HPC1 and HPC2 populations (**Figure 6, A and B**). While EpCAM expression was nearly extinguished during differentiation to CMP, GMP, MEP committed progenitors, it was upregulated in terminally differentiated cells (myeloid, B, and T lineages) from PB (**Figure 6B**). EpCAM positive HSPCs from *Zeb1*$^{-/-}$ LSKs expanded more than their

EpCAM negative counterparts *in vitro* (**Figure 6C)**, suggesting that EpCAM expression confers a cell survival signal in *Zeb1*$^{-/-}$ HSCs. We directly addressed whether EpCAM expression mediates cell survival in freshly isolated *Zeb1*$^{-/-}$ HSCs and *in vitro* and observed reduced apoptosis in *Zeb1*$^{-/-}$ *EpCAM*$^{+}$ HSCs and multipotent progenitor subsets in both settings (**Figure 6, D and E**). Cell cycle status based on EpCAM expression was unperturbed in *Zeb1*$^{-/-}$ HSCs (**Figure 6F**). By evaluating the impact of EpCAM expression in *Zeb1*$^{-/-}$ HSC survival and differentiation *in vivo*, we showed at 16 weeks after HSC transplantation that *Zeb1*$^{-/-}$ cells in PB displayed a 2-fold increase in EpCAM expression compared to controls (**Figure 6G**). Thus, EpCAM expression in *Zeb1*$^{-/-}$ HSC correlates with the multi-lineage differentiation block observed during transplantation (**Figure 3 and 4**). Yet, high expression of EpCAM was preserved in *Zeb1*$^{-/-}$ HSPCs at 16 weeks after transplant and these *EpCAM*$^{+}$ *Zeb1*$^{-/-}$ HSPCs had a lower propensity for apoptosis (**Figure 6, H and I**). Together, these data suggest that augmented EpCAM expression confers a cell survival advantage in *Zeb1*$^{-/-}$ HSCs that causes an imbalance between self-renewal and differentiation fates.

Zeb1$^{-/-}$ *EpCAM*$^{+}$ HSPCs display enhanced cell survival and diminished mitochondrial metabolism, RNA biogenesis and differentiation transcriptional signatures

To evaluate the transcriptomic signature demarcating *Zeb1*$^{-/-}$ *EpCAM*$^{+}$ HSPCs from *Zeb1*$^{-/-}$ *EpCAM*$^{-}$ HSPCs, we performed RNA sequencing on *Zeb1*$^{-/-}$ *EpCAM*$^{+}$ LSK cells or *Zeb1*$^{-/-}$ *EpCAM*$^{-}$ LSK cells 14 days after the last dose of pIpC. 3263 genes were up-regulated and 3153 genes were down-regulated in

Zeb1$^{-/-}$ *EpCAM*$^{+}$ HSPCs (**Figure 7A**). In agreement with enhanced cell survival and a functional block in differentiation associated with *Zeb1*$^{-/-}$ *EpCAM*$^{+}$ HSCs (**Figure 6**), biological pathway analysis revealed a robust p53 mediated pro-survival signature and an anti-hematopoietic differentiation signature in *Zeb1*$^{-/-}$ *EpCAM*$^{+}$ HSPCs (**Figure 7, B-D**). Furthermore, we observed augmented expression of anti-apoptotic BCL-XL (54) in *Zeb1*$^{-/-}$ *EpCAM*$^{+}$ HSPCs (**Figure 7, C and E**), and an EpCAM-p53-BCL-XL (BCL2L1) interacting gene network of apoptotic regulation in *Zeb1*$^{-/-}$ HSPCs (**Supplemental Figure 6**).

Mitochondria play crucial regulatory roles in fundamental cellular processes, such as apoptosis and bioenergetic provisions (55) and in the context of HSCs act as a gatekeeper limiting HSC self-renewal ability (56). *Zeb1*$^{-/-}$ *EpCAM*$^{+}$ HSPC displayed reduced mitochondrial gene expression, transport, translation and protein import as well as reduced associated mitochondrial metabolic pathways (e.g. pyruvate metabolism and TCA cycle) critical to HSC fate (57) **(Figure 7F**). Further highlighting the relatively low bioenergetic state of *Zeb1*$^{-/-}$ *EpCAM*$^{+}$ HSPCs, ribosome biogenesis, and ribosome associated pathways, such as rRNA processing, whose reduction has previously been associated with conferral of stress resistance in pre-leukemic HPSCs (58), were similarly downregulated in *Zeb1*$^{-/-}$ *EpCAM*$^{+}$ HSPCs (**Figure 7F**). Consistent with this, *Zeb1*$^{-/-}$ *EpCAM*$^{+}$ HSPCs also displayed augmented acute myeloid leukemia signaling (**Figure 7F**). Therefore, in addition to control of cell survival, *Zeb1* mediated repression of EpCAM appears to be critical in regulating mitochondrial metabolism and ribosomal pathways associated with normal HSC maintenance and prevention of pre-leukemic and leukemic signaling.

ZEB1 expression is downregulated in AML patients and acute deletion of *Zeb1* in LSCs enhances disease progression in *MLL-AF9* and *Meis1a/Hoxa9* driven AML

Subversion of HSC fates may cause hematologic neoplasia, including leukemia (59)**.** Having found that *Zeb1* deficiency leads to critical impairments in HSC self-renewal, apoptotic and differentiation fates and because increased EpCAM expression in *Zeb1* deficient HSCs enhanced AML signaling, we assessed the role of *Zeb1* in AML. We initially evaluated ZEB1 expression in a large cohort of AML patients. AML (n = 2611) and control (n = 77) patient datasets were obtained from Gene Expression Omnibus (GEO) to assemble a case/control cohort hybridized to Affymetrix Human Genome U133 Plus 2.0 GeneChip array and analyzed through R using bio-conductor packages, where data was normalized using Robust Multi-array Average (RMA). We observed that ZEB1 expression was lower in AML patients compared to healthy controls (**Figure 8A**). Attenuated expression of ZEB1 was particularly prevalent in M4 and M5 FAB subtypes and, also in AML patients with t(8;21) and *MLL* chromosomal translocations (60, 61) (**Figure 8, B and C**). Using an independent AML patient database (www.bloodspot.eu), we validated lower ZEB1 expression in patients harboring these chromosomal translocations (**Figure 8D**).

While these data imply that *ZEB1* acts as a tumor suppressor in AML, the functional requirement of *Zeb1* in AML disease progression remains unknown. To directly assess this, we employed an assay in which leukemic transformation of murine C-KIT+ HSPCs is mediated by retroviral

overexpression of either *MLL-AF9* or *Meis1a/Hoxa9* AML oncogenes (62-64). *MLL-AF9* or *Meis1a/Hoxa9*-transduced cells were serially passaged for three rounds in CFCs to generate pre-LSCs, which, on intravenous injection into primary lethally irradiated mice, become LSCs – the malignant counterparts of HSCs that drive disease progression in AML (65) (**Figure 8E**). We co-transduced HSPCs from non-induced *Zeb1*$^{fl/fl}$*;Mx1-Cre*$^{+}$ or control mice with retroviruses expressing either *MLL-AF9* or *Meis1a/Hoxa9*, collected pre-LSCs and transplanted them into primary recipients alongside unfractionated BM support cells (**Figure 8E**). By flow cytometry, we assessed the PB of recipients for engrafting leukemic cells and induced *Zeb1* deletion with pIpC after disease onset, when 20% engraftment of leukemic cells was observed in the PB (66) **(**data not shown). In both *MLL-AF9* and *Meis1a/Hoxa9* leukemic models, recipients of *Zeb1* KO LSCs succumbed to AML with enhanced rapidity compared to recipients receiving control LSCs, indicating that *Zeb1* deletion accelerates LSC mediated disease progression (**Figure 8, F and G**). Thus, *Zeb1* acts as a tumor suppressor in *MLL-AF9* and *Meis1a/Hoxa9* AML LSCs.

Discussion

Zeb1, in its capacity as a critical EMT regulator, controls myriad processes in embryonic development, and through the agency of tissue-specific stem cells, acts as a critical regulator of adult tissue homeostasis (18). Deregulation of *Zeb1* activity has been implicated in multiple cancer types and, in these settings, *Zeb1* acts as an instigator of the activity of cancer stem cells, a subset of cancer cells driving therapy resistance and metastasis, which ultimately cause fatality (42, 43). Understanding the cellular and molecular mechanisms underpinning *Zeb1* mediated regulation of stem cell self-renewal, lineage fate and differentiation in normal and cancer stem cells remains incomplete. Here, in stem cells of the hematopoietic system, we find that acute conditional deletion of *Zeb1* causes a profound cell-autonomous self-renewal defect and differentiation block across all lineages after transplantation and deregulates a transcriptional program associated with cell polarity. Strikingly, acute conditional deletion of *Zeb1* in HSCs and their progeny affects the lineage fate and cell survival of T cells, leading to a rapid loss of thymocytes and $CD8^+$ T-cell subsets.

While it is known that *Zeb1* and other transcription factors, such as zinc finger transcription factor *Gata3*, are essential in T-cell development (67, 68), the process in adults is less clear. Here we identify *Zeb1* as an indispensable regulator of transcriptional programming for the entire adult T-cell repertoire, during initial T-cell commitment from HSPC bone marrow progenitor subsets through to cell survival during positive and negative selection in the thymus. In

spite of incomplete gene deletion using the *Mx-Cre* system, we also identified *Zeb1* as a regulator of $CD8^+$ EM in BM and PB and $CD8^+$ CM T cells from spleen, supporting previous observations that *Zeb1* is critical to $CD8^+$ T cell function during infection (69). Our data are also consistent with the notion that the ZEB family member *Zeb2* plays reciprocal roles in $CD8^+$ T cell biology (69) and that it does not compensate for the absence of *Zeb1*. Further understanding *Zeb1* mediated control of adult T-cell differentiation may have implications for immunosurveillance, a naturally occurring immune mechanism involving $CD8^+$ T cells and other immune subsets that eradicate tumor cells (70, 71). In particular, the complex interplay between the necessity for *Zeb1* in immune cell subsets involved in immunosurveillance and the tumor microenvironment, where paradoxically ZEB1 expression can drive metastasis by interfering with immune checkpoints, requires further exploration to negate possible toxic effects associated with targeting ZEB1 or ZEB1 target genes therapeutically in cancer. Nonetheless, the benefits of modulating the *Zeb1* transcriptional/epigenetic network in cancer immunotherapy have been clearly illustrated in the blockade of CD47, a direct transcriptional target of *Zeb1*, that enhances phagocytosis of breast cancer cells undergoing EMT (72).

Zeb1$^{-/-}$ HSCs were functionally defective in their capacity to generate other blood lineages in transplantation, suggesting that *Zeb1* modulates the ability of HSCs to differentiate correctly *in vivo* through repression of lineage-commitment affiliated gene programs in HSCs. In keeping with the notion of lineage specific transcriptional repression licensed by *Zeb1*, we observed upregulation of 79% of genes in *Zeb1*$^{-/-}$ HSCs together with a robust gene

expression signature associated with de-regulated multi-lineage differentiation. Relatively few transcriptional repressors, including *Gfi1* and *Gfi1b*, have been shown to regulate HSC self-renewal and differentiation function (73). *Gfi1*$^{-/-}$ HSCs have a phenotype resembling that observed in *Zeb1*$^{-/-}$ HSCs (74, 75) and, notably, both *Gfi1* and *Gfi1b* were transcriptionally repressed in *Zeb1*$^{-/-}$ HSCs, suggesting positive regulation by ZEB1. *Zeb1* therefore likely acts as a transcriptional repressor that regulates HSC self-renewal and global differentiation *via* a transcriptional repressor network that includes both *Gfi1* and *Gfi1b*.

Zeb1 regulates HSC self-renewal and differentiation in association with a transcriptional program of cell polarity, which relates to the structural and cellular changes that occur to a cell, facilitating specialized function, such as cell division, adhesion or migration (76). Several studies in *Drosophila melanogaster* male germline stem cells (77, 78) support the long-standing hypothesis that cell polarity acts as a critical mechanism that asserts control of symmetric versus asymmetric stem cell division and therefore stem cell fate; simply put, striking a balance between self-renewal and differentiation fates in tissue homeostasis and under conditions of physiologic stress (76, 79). Notably, *Numb*, a marker of asymmetric division in *Drosophila melanogaster* neuroblasts (80), and *Crb3*, which asymmetrically distributes polarity proteins in mouse preimplantation embryos (81) were deregulated in *Zeb1*$^{-/-}$ HSCs. Taken together with the observation that *Zeb1*$^{-/-}$ HSCs have decreased self-renewal potential, these data suggesting that *Zeb1*$^{-/-}$ HSCs favor symmetric, differentiating divisions over asymmetric divisions. Other regulators of cell

polarity, including genes associated with apical-basal polarity (82), such as tight-junctions (*Ocln, Marveld2, Tjp3*), adherens junctions (*Cdh1*) and desmosomes (*Krt8, Dsc2, Dsg2*), were upregulated in *Zeb1*$^{-/-}$ HSCs. We provide evidence that de-repression of EpCAM in *Zeb1*$^{-/-}$ HSCs correlates with enhanced HSC survival in homeostasis and transplantation. Yet, enhanced HSC survival and relative upregulation of EpCAM in PB correlates with a block in engraftment in transplantation of *Zeb1*$^{-/-}$ HSCs, suggesting that enhanced survival of HSCs mediated by EpCAM disturbs the delicate balance of self-renewal versus differentiation fates.

EpCAM expression in *Zeb1*$^{-/-}$ HSCs reduced mitochondrial metabolism, which is also important for HSC self-renewal, cell survival and differentiation fates (57). For example, reduced pyruvate metabolism was observed in *EpCAM*$^{+}$ *Zeb1*$^{-/-}$ HSPCs, which is consistent with evidence that ablating aspects of pyruvate metabolism causes HSC exhaustion and a block in HSC differentiation (83, 84). Associated with a low metabolic state, *EpCAM*$^{+}$ *Zeb1*$^{-/-}$ HSPCs also exhibited reduced ribosome biogenesis, which may reflect enhanced cell survival mediated by the combinatorial lack of p53 target gene phosphorylation, stabilization of p53 and reduced rRNA observed in *EpCAM*$^{+}$ *Zeb1*$^{-/-}$ HSPCs (58, 85). In future work, it will be of interest to further evaluate the genetic requirement for EpCAM in *Zeb1* mediated HSC function in the context of mitochondrial metabolism and ribosome biogenesis.

Deregulation of cell adhesion molecules or other cell polarity genes, such as EpCAM, which are a normal feature of epithelial cells, could also be

incompatible with the predominantly mesenchymal milieu of the BM environment and may facilitate aberrant, cell-autonomous driven interactions of HSCs with components of the BM niche (86) . This could restrain the motility or alter survival and quiescence of HSCs (or HSPC subsets) within the BM. Studies should be conducted utilizing *in vivo* imaging of *Zeb1*$^{-/-}$ HSCs in their BM habitat to define the broader role of cell polarity related molecules in vascular and osteoblastic BM niches and how they might influence HSC fate.

Perturbation of cell polarity is also a hallmark of cancer development (87) and given our findings of *Zeb1's* impact on myeloid differentiation – which is blocked in AML – we explored the function of *Zeb1* in AML. In hematologic malignancies *Zeb1* has variably been reported as either a tumor suppressor (in Sézary syndrome and adult T-cell leukemia/lymphoma) (88-90) or an oncogene (in mantle cell lymphoma) (91). We found *ZEB1* expression was reduced in select AML patient subtypes, including those involving *MLL* chromosomal translocations that confer poor prognosis in AML (92). Induction of *Zeb1 KO* in LSC mouse models of *MLL-AF9* and *Meis1a/Hoxa9*-driven AML accelerated disease progression, implying that *Zeb1* acts as a tumor suppressor in AML LSCs. In support of this, ablating pro-oncogenic *Gata2* in AML LSCs caused upregulation of *Zeb1* expression (66). Taken together with analysis of *Zeb1*$^{-/-}$ HSCs, these data suggest that *Zeb1* mediated control of HSC self-renewal, apoptosis and differentiation fates is integral to suppressing their vulnerability to leukemic transformation and disease progression in AML. This view is in agreement with the likely pre-leukemic selective advantage provided by decreased ribosome biogenesis (58) and enhanced AML signaling in *Zeb1*$^{-/-}$

EpCAM^{+} HSPCs. To the contrary, however, and consistent with an oncogenic function for *Zeb1* in AML, high expression of *Zeb1* has been found to drive dissemination of AML LSCs and leukemic cells to extramedullary sites and other organs (92). Yet, the cell context dependent requirement for *Zeb1* in initiating and propagating AML (93) remains ambiguous and requires further in-depth experimentation.

Methods and Materials

Mice

We have generated *Zeb1*$^{fl/fl}$ mice (23) which were bred with *Mx1-Cre*$^{+/-}$ mice (25) to generate an experimental cohort of *Zeb1*$^{fl/fl}$ *Mx1-Cre*$^{-/-}$ (control) and *Zeb1*$^{fl/fl}$ *Mx1-Cre*$^{+/-}$ (*Zeb1*$^{-\backslash-}$). *Zeb1* was deleted after intraperitoneal (IP) administration of Polyinosinic:polycytidylic acid (pIpC) (6 doses every alternate day, 0.3 mg per dose, GE Healthcare). All experiments were performed under the regulations of the UK Home Office. Genotyping is described in Supplemental Methods.

Flow cytometry analysis

Bones (femurs, tibias, iliac bones) were crushed using a pestle and mortar in phosphate-buffered saline (PBS) supplemented with 2% fetal bovine serum (FBS) and the BM cell suspension was filtered through 70 μm cell strainer (Miltenyi Biotec). Spleen and thymi were minced through 70 μm cell strainer to obtain a homogeneous cell suspension. PB was obtained from the tail vein in EDTA treated tubes (Starstedt). Red blood cells were lysed by ammonium chloride solution (StemCellTechnologies). For the immunophenotypic analysis, cells were stained as follows: for HSPCs (LSK SLAM): Lineage cocktail was prepared from a pool of biotinylated antibodies of differentiated cell markers in PBS 2% FBS (MAC1 and GR1 for myeloid cells, TER119 for erythroid lineage, B220 for B cells, CD3e, CD4, CD8a for T cells), SCA-1-APCCy7, C-KIT-APC, CD150-PECy7, and CD48-FITC to study HSC, MPP, HPC1, and HPC2; for the committed progenitors (LK) LIN cocktail as in LSK SLAM, SCA-1-APCCy7,

CKIT-APC, CD34-FITC, CD16/32-PECy7, CD135-PE, and CD127-BV650 to study LMPP, CMP, GMP, MEP, and CLP. The lineage cocktail was detected by adding streptavidin as a secondary antibody. Lineage positive cells from the BM and spleen were stained for GR1-PECy7 and MAC1-APC (myeloid cells), CD3-APC, CD4-PE, CD8-APCCy7 (T-cells), B220-FITC (B-cells), CD62L-PECy7, CD44-APC (naïve, effector, and memory T cells). For thymocytes, cells were stained for CD4 and CD8, CD44, CD25 and C-KIT to study early and late stages of T cell development in thymus. For apoptosis assay, after staining the cells for cell surface markers, they were stained with Annexin V-PE antibody (BioLegend) for 30 minutes in the dark at RT and diamidino-2-phenylindole (DAPI 1 µg/ml) (Molecular probes) was added before running the samples. Ki67 for cell cycle analysis in HSCs and intracellular staining were done after the extracellular staining, the cells were fixed in 1% paraformaldehyde (PFA) (ThermoFisher) for 20 minutes at 4^{o}C, permeabilized using PBS containing 0.1% Saponin (Sigma) for 30 minutes at 4^{o}C, and then stained with the antibodies for 30 minutes at 4^{o}C in dark. For cell cycle, cells were incubated with DAPI at final concentration of 5 ug/mL in dark for 5 minutes before running the samples. Samples were analyzed using BD LSRFortessa^{TM} (BD Biosciences). Data were analyzed using FlowJo 10.0.8 (Tree Star, Inc). A full list of antibodies used is shown Supplemental Table 1.

For HSC sorting, BM cell suspension was obtained and red blood cells were lysed by ammonium chloride solution (StemCellTechnologies). Cells were enriched for CKIT by magnetic-activated cell sorting (MACS) (MACS®, Miltenyi Biotec) using anti-CKIT magnetic beads (Miltenyi Biotec). CKIT^{+} cells were

stained as described earlier and HSCs were sorted using a BD FACSAria™ Fusion (BD Biosciences).

Transplantation experiments

C57BL/6 SJL mice (CD45.1) were used as recipients for all the transplantations except for the niche transplantation C57BL/6 (CD45.2) mice (The Jackson Laboratory, Bar Harbor, ME USA) were used as recipients. The mice were lethally irradiated at 9 Gy (split dose). For primary transplantation, 150 HSCs from *Zeb1*$^{-/-}$ and control cells mixed with 2X10^5 whole BM (CD45.1) (supporting cells) were intravenously transplanted into lethally irradiated mice (CD45.1). To monitor the engraftment, tail vein bleeding was performed at different time points post-transplant. To further assess the capacity of Zeb1-deficient HSCs to repopulate secondary recipients, 300 HSCs from *Zeb1*$^{-/-}$ and control mixed with 3 x10^5 whole BM (CD45.1) (supporting cells) were intravenously transplanted into lethally irradiated mice (CD45.1). The engraftment ability was monitored via tail vein bleeding as was done with the primary recipients.

For cell autonomous transplantation, *Zeb1* was deleted specifically in hematopoietic cells (but not in BM niche cells) after transplanting 5X10^5 whole BM (CD45.2) from *Zeb1*$^{fl/fl}$ *Mx1-Cre*$^+$ and *Zeb1*$^{fl/fl}$ *Mx1-Cre*$^-$ along with 5X10^5 whole BM (CD45.1) (supporting cells) into lethally irradiated recipients (CD45.1). Six weeks later, 6 doses of pIpC (every alternate day, 0.3 mg per dose) were intraperitoneally (IP) injected to delete *Zeb1*. Mice were dissected at day 14 after the last dose of pIpC and analyzed. For the cell autonomous secondary transplantation, 5x10^5 CD45.2 donor BM cells were sorted from

control and *Zeb1*$^{-/-}$ primary recipients and mixed with competitor cells and re-transplanted into lethally irradiated recipients.

For niche transplantation, 1 x10^6 total BM cells from wild type CD45.1$^+$ mice were transplanted into lethally irradiated *Zeb1*$^{fl/fl}$ *Mx1-Cre*$^+$ and *Zeb1*$^{fl/fl}$ *Mx1-Cr*$^-$ mice. Six weeks later, 6 doses of (every alternate day, 0.3 mg per dose) were IP injected to delete *Zeb1*. Mice were dissected at week 16 after the last dose of pIpC.

Leukemia transformation assay

1X10^6 CD45.2$^+$ C-KIT$^+$ cells were obtained from control and Zeb1$^{fl/fl}$ Mx1-Cre$^{-/+}$ mice and cultured in IMDM 10% FBS supplemented with 40 ng/mL SCF, 20 ng/mL IL-3, and 20 ng/mL IL-6. The next day, the cells were transduced with retroviral vectors encoding Meis1a/Hoxa9 and MLL-AF9 using retronectin-coated plates (TaKaRa) as described previously (64, 66). After 72 hours, 5,000 cells were plated in colony forming units assay 1 (CFC1) using MethoCult™ M3231 (STEMCELL Technologies) semi-solid media for 6 days and this process repeated for up to 3 rounds of CFCs. At the end of CFC3, pre-LSCs were harvested and sorted according to C-KIT expression and transplanted into lethally-irradiated primary recipients. Three weeks later, *Zeb1* was deleted after IP administration of pIpC (8 doses every alternate day, 0.3 mg per dose, GE Healthcare). Mice were monitored for AML development.

RNA-sequencing

RNA from HSCs (LSK CD150$^+$ CD48$^-$) and CLP (LIN$^-$ SCA-1^{low} C-KIT^{low}

CD127^{+}) from control and *Zeb1*$^{-/-}$ mice 14 days after the last dose of pIpC injection was extracted using RNAeasy micro kit (Qiagen). Total RNA quality and quantity was assessed using Agilent 2100 Bioanalyzer and RNA Nano 6000 kit (Agilent Technologies). The library was prepared using the NEB® Ultra™ II Directional RNA Library Prep Kit for Illumina® (NEB). The libraries then were sequenced using a 75-base paired-end (2x75bp PE) dual index read format on the Illumina® HiSeq4000 according to the manufacturer's instructions. Further details on sequencing and bioinformatics were described previously (66).

The heatmap was created using Morpheus, an online tool, (Broad Institute). Differentially expressed genes (DEGs) according to FDR <0.05 were used for heatmaps. The biological pathway analysis was performed using BioCarta, KEGG and Reactome pathway databases run on GSEA software (94) as well as Ingenuity Pathway Analysis software (IPA) (QIAGEN Inc., https://www.qiagenbioinformatics.com/products/ingenuity-pathwayanalysis).
IPA was used to create a prediction network of Zeb1 interactions with its target genes.

RNA sequencing for EPCAM+ and EPCAM- from *Zeb1*$^{-/-}$ mice is described in Supplemental Methods.

All RNA-sequencing data can be accessed at the GEO (GSE153664, GSE154615).

AML patients bioinformatic analysis

A cohort of 2611 AML and 77 control were obtained from GEO (GSE14468, GSE22845, GSE10358, GSE12417, GSE13159, GSE14062, GSE15434, GSE16015, GSE38987, GSE22056, GSE33223, GSE17855, GSE15389) (95) and ArrayExpress (E-MTAB-3444) (96). R software was used to analyze and produce data. Data processing, normalization, and analysis were described previously (97).

Statistical Analysis

Figures were prepared using Prism (GraphPad Software, Inc.). Statistical analyses were done using Mann–Whitney U test to calculate significance as follows: *P < .05, **P < .01, ***P < .001, ****P <0.0001.

Study Approval

All animal experiments were performed according to protocols ratified by the UK Home Office and carried out at Cardiff University animal facility under project number 30/3380.

Author Contributions

A. Almotiri designed and performed experiments, analyzed and interpreted the data, prepared the figures, and contributed to writing the manuscript. H.A contributed to experimental design, performed experiments, analyzed and interpreted the data, analyzed RNA-Seq data and reviewed the manuscript. J.B.M.-G. contributed to experimental design, performed experiments, analyzed and interpreted the data, and reviewed the manuscript. A. Abdelfattah and B.A. performed experiments, analyzed data and reviewed the manuscript. L.S., A.G, M.G, A.G, A. Alsayari, S.T, L.T, D.S performed experiments and contributed to data analysis. S.E. and P.G. performed bioinformatics analyses. M.P.S, S.B, T.B contributed to experimental design/analysis and reviewed the manuscript. A.S.B. and F.S contributed significantly to experimental design, data analysis/interpretation and to manuscript preparation. N.P.R. conceived and supervised the project, designed experiments, analyzed and interpreted the data, and wrote the manuscript.

Acknowledgements

Supported by the British Society for Hematology, Life Science Research Network Wales, Leukemia Cancer Society, Leukemia Research Appeal for Wales and the Lady Tata Memorial Trust (to N.P.R). We thank Shelley Rundle for assistance with RNA-sequencing and Robert Andrews assistance with bioinformatics. The graphical abstract was drawn using BioRender.

Conflict of interest statement

The authors declare no conflict of financial interest

References

1. Nieto MA, Huang RY, Jackson RA, and Thiery JP. EMT: 2016. *Cell.* 2016;166(1):21-45.
2. Kalluri R, and Weinberg RA. The basics of epithelial-mesenchymal transition. *J Clin Invest.* 2009;119(6):1420-8.
3. Postigo AA, and Dean DC. ZEB, a vertebrate homolog of Drosophila Zfh-1, is a negative regulator of muscle differentiation. *The EMBO journal.* 1997;16(13):3935-43.
4. Postigo AA, Ward E, Skeath JB, and Dean DC. zfh-1, the Drosophila homologue of ZEB, is a transcriptional repressor that regulates somatic myogenesis. *Mol Cell Biol.* 1999;19(10):7255-63.
5. Jethanandani P, and Kramer RH. Alpha7 integrin expression is negatively regulated by deltaEF1 during skeletal myogenesis. *J Biol Chem.* 2005;280(43):36037-46.
6. Postigo AA, and Dean DC. Independent repressor domains in ZEB regulate muscle and T-cell differentiation. *Mol Cell Biol.* 1999;19(12):7961-71.
7. Clark SG, and Chiu C. C. elegans ZAG-1, a Zn-finger-homeodomain protein, regulates axonal development and neuronal differentiation. *Development.* 2003;130(16):3781-94.
8. Jiang Y, Yan L, Xia L, Lu X, Zhu W, Ding D, et al. Zinc finger E-box-binding homeobox 1 (ZEB1) is required for neural differentiation of human embryonic stem cells. *J Biol Chem.* 2018;293(50):19317-29.
9. Singh S, Howell D, Trivedi N, Kessler K, Ong T, Rosmaninho P, et al. Zeb1 controls neuron differentiation and germinal zone exit by a mesenchymal-epithelial-like transition. *Elife.* 2016;5:e12717.
10. Wang H, Xiao Z, Zheng J, Wu J, Hu XL, Yang X, et al. ZEB1 Represses Neural Differentiation and Cooperates with CTBP2 to Dynamically Regulate Cell Migration during Neocortex Development. *Cell Rep.* 2019;27(8):2335-53.e6.
11. Funahashi J, Sekido R, Murai K, Kamachi Y, and Kondoh H. Delta-crystallin enhancer binding protein delta EF1 is a zinc finger-homeodomain protein implicated in postgastrulation embryogenesis. *Development.* 1993;119(2):433-46.
12. Higashi Y, Moribe H, Takagi T, Sekido R, Kawakami K, Kikutani H, et al. Impairment of T cell development in deltaEF1 mutant mice. *J Exp Med.* 1997;185(8):1467-79.
13. Takagi T, Moribe H, Kondoh H, and Higashi Y. DeltaEF1, a zinc finger and homeodomain transcription factor, is required for skeleton patterning in multiple lineages. *Development.* 1998;125(1):21-31.
14. Brabletz T, Jung A, Spaderna S, Hlubek F, and Kirchner T. Opinion: migrating cancer stem cells - an integrated concept of malignant tumour progression. *Nat Rev Cancer.* 2005;5(9):744-9.
15. Shibue T, and Weinberg RA. EMT, CSCs, and drug resistance: the mechanistic link and clinical implications. *Nat Rev Clin Oncol.* 2017;14(10):611-29.
16. Goossens S, Vandamme N, Van Vlierberghe P, and Berx G. EMT transcription factors in cancer development re-evaluated: Beyond EMT and MET. *Biochim Biophys Acta Rev Cancer.* 2017;1868(2):584-91.

17. Berx G, Raspe E, Christofori G, Thiery JP, and Sleeman JP. Pre-EMTing metastasis? Recapitulation of morphogenetic processes in cancer. *Clin Exp Metastasis.* 2007;24(8):587-97.
18. Brabletz S, and Brabletz T. The ZEB/miR-200 feedback loop--a motor of cellular plasticity in development and cancer? *EMBO Rep.* 2010;11(9):670-7.
19. Wellner U, Schubert J, Burk UC, Schmalhofer O, Zhu F, Sonntag A, et al. The EMT-activator ZEB1 promotes tumorigenicity by repressing stemness-inhibiting microRNAs. *Nat Cell Biol.* 2009;11(12):1487-95.
20. Siebzehnrubl FA, Silver DJ, Tugertimur B, Deleyrolle LP, Siebzehnrubl D, Sarkisian MR, et al. The ZEB1 pathway links glioblastoma initiation, invasion and chemoresistance. *European Molecular Biology Organization Molecular Medicine.* 2013;5(8):1196-212.
21. Singh DK, Kollipara RK, Vemireddy V, Yang XL, Sun Y, Regmi N, et al. Oncogenes Activate an Autonomous Transcriptional Regulatory Circuit That Drives Glioblastoma. *Cell Rep.* 2017;18(4):961-76.
22. Li G, Luo W, Abdalla BA, Ouyang H, Yu J, Hu F, et al. miRNA-223 upregulated by MYOD inhibits myoblast proliferation by repressing IGF2 and facilitates myoblast differentiation by inhibiting ZEB1. *Cell Death Dis.* 2017;8(10):e3094.
23. Brabletz S, Lasierra Losada M, Schmalhofer O, Mitschke J, Krebs A, Brabletz T, et al. Generation and characterization of mice for conditional inactivation of Zeb1. *Genesis (New York, NY : 2000).* 2017;55(4).
24. Postigo AA, and Dean DC. Differential expression and function of members of the zfh-1 family of zinc finger/homeodomain repressors. *Proc Natl Acad Sci U S A.* 2000;97(12):6391-6.
25. Kuhn R, Schwenk F, Aguet M, and Rajewsky K. Inducible gene targeting in mice. *Science.* 1995;269(5229):1427-9.
26. Lagasse E, and Weissman IL. Flow cytometric identification of murine neutrophils and monocytes. *J Immunol Methods.* 1996;197(1-2):139-50.
27. Sunderkotter C, Nikolic T, Dillon MJ, Van Rooijen N, Stehling M, Drevets DA, et al. Subpopulations of mouse blood monocytes differ in maturation stage and inflammatory response. *J Immunol.* 2004;172(7):4410-7.
28. Bhandoola A, and Sambandam A. From stem cell to T cell: one route or many? *Nat Rev Immunol.* 2006;6(2):117-26.
29. Godfrey DI, Kennedy J, Suda T, and Zlotnik A. A developmental pathway involving four phenotypically and functionally distinct subsets of CD3-CD4-CD8- triple-negative adult mouse thymocytes defined by CD44 and CD25 expression. *J Immunol.* 1993;150(10):4244-52.
30. Matsuzaki Y, Gyotoku J, Ogawa M, Nishikawa S, Katsura Y, Gachelin G, et al. Characterization of c-kit positive intrathymic stem cells that are restricted to lymphoid differentiation. *J Exp Med.* 1993;178(4):1283-92.
31. Ceredig R, and Rolink T. A positive look at double-negative thymocytes. *Nature Reviews Immunology.* 2002;2(11):888.
32. Allman D, Sambandam A, Kim S, Miller JP, Pagan A, Well D, et al. Thymopoiesis independent of common lymphoid progenitors. *Nat Immunol.* 2003;4(2):168.

33. Bhandoola A, Sambandam A, Allman D, Meraz A, and Schwarz B. Early T lineage progenitors: new insights, but old questions remain. *J Immunol.* 2003;171(11):5653-8.
34. Zhang J, Niu C, Ye L, Huang H, He X, Tong WG, et al. Identification of the haematopoietic stem cell niche and control of the niche size. *Nature.* 2003;425(6960):836-41.
35. Ghaedi M, Steer CA, Martinez-Gonzalez I, Halim TYF, Abraham N, and Takei F. Common-Lymphoid-Progenitor-Independent Pathways of Innate and T Lymphocyte Development. *Cell Rep.* 2016;15(3):471-80.
36. Adolfsson J, Mansson R, Buza-Vidas N, Hultquist A, Liuba K, Jensen CT, et al. Identification of Flt3+ lympho-myeloid stem cells lacking erythro-megakaryocytic potential a revised road map for adult blood lineage commitment. *Cell.* 2005;121(2):295-306.
37. Pietras EM, Reynaud D, Kang YA, Carlin D, Calero-Nieto FJ, Leavitt AD, et al. Functionally Distinct Subsets of Lineage-Biased Multipotent Progenitors Control Blood Production in Normal and Regenerative Conditions. *Cell Stem Cell.* 2015;17(1):35-46.
38. Oguro H, Ding L, and Morrison SJ. SLAM family markers resolve functionally distinct subpopulations of hematopoietic stem cells and multipotent progenitors. *Cell Stem Cell.* 2013;13(1):102-16.
39. Mooney CJ, Cunningham A, Tsapogas P, Toellner KM, and Brown G. Selective Expression of Flt3 within the Mouse Hematopoietic Stem Cell Compartment. *Int J Mol Sci.* 2017;18(5):1037.
40. Sitnicka E, Bryder D, Theilgaard-Monch K, Buza-Vidas N, Adolfsson J, and Jacobsen SE. Key role of flt3 ligand in regulation of the common lymphoid progenitor but not in maintenance of the hematopoietic stem cell pool. *Immunity.* 2002;17(4):463-72.
41. Kumar R, Fossati V, Israel M, and Snoeck HW. Lin-Sca1+kit- bone marrow cells contain early lymphoid-committed precursors that are distinct from common lymphoid progenitors. *J Immunol.* 2008;181(11):7507-13.
42. Zhang P, Sun Y, and Ma L. ZEB1: at the crossroads of epithelial-mesenchymal transition, metastasis and therapy resistance. *Cell Cycle.* 2015;14(4):481-7.
43. Aigner K, Dampier B, Descovich L, Mikula M, Sultan A, Schreiber M, et al. The transcription factor ZEB1 (deltaEF1) promotes tumour cell dedifferentiation by repressing master regulators of epithelial polarity. *Oncogene.* 2007;26(49):6979-88.
44. Sanchez-Tillo E, Lazaro A, Torrent R, Cuatrecasas M, Vaquero EC, Castells A, et al. ZEB1 represses E-cadherin and induces an EMT by recruiting the SWI/SNF chromatin-remodeling protein BRG1. *Oncogene.* 2010;29(24):3490-500.
45. Vannier C, Mock K, Brabletz T, and Driever W. Zeb1 regulates E-cadherin and Epcam (epithelial cell adhesion molecule) expression to control cell behavior in early zebrafish development. *J Biol Chem.* 2013;288(26):18643-59.
46. Gonzalez B, Denzel S, Mack B, Conrad M, and Gires O. EpCAM is involved in maintenance of the murine embryonic stem cell phenotype. *Stem Cells.* 2009;27(8):1782-91.

47. Chapple RH, Tseng YJ, Hu T, Kitano A, Takeichi M, Hoegenauer KA, et al. Lineage tracing of murine adult hematopoietic stem cells reveals active contribution to steady-state hematopoiesis. *Blood Advances.* 2018;2(11):1220-8.
48. Bendriem RM, Singh S, Aleem AA, Antonetti DA, and Ross ME. Tight junction protein occludin regulates progenitor Self-Renewal and survival in developing cortex. *Elife.* 2019;8.
49. Bierie B, Pierce SE, Kroeger C, Stover DG, Pattabiraman DR, Thiru P, et al. Integrin-β4 identifies cancer stem cell-enriched populations of partially mesenchymal carcinoma cells. *Proc Natl Acad Sci U S A.* 2017;114(12):E2337-e46.
50. Phillips JL, Taberlay PC, Woodworth AM, Hardy K, Brettingham-Moore KH, Dickinson JL, et al. Distinct mechanisms of regulation of the ITGA6 and ITGB4 genes by RUNX1 in myeloid cells. *J Cell Physiol.* 2018;233(4):3439-53.
51. Postigo AA, and Dean DC. ZEB represses transcription through interaction with the corepressor CtBP. *Proc Natl Acad Sci U S A.* 1999;96(12):6683-8.
52. Purbey PK, Singh S, Notani D, Kumar PP, Limaye AS, and Galande S. Acetylation-dependent interaction of SATB1 and CtBP1 mediates transcriptional repression by SATB1. *Mol Cell Biol.* 2009;29(5):1321-37.
53. Schnell U, Cirulli V, and Giepmans BN. EpCAM: structure and function in health and disease. *Biochim Biophys Acta.* 2013;1828(8):1989-2001.
54. Rodrigues NP, Janzen V, Forkert R, Dombkowski DM, Boyd AS, Orkin SH, et al. Haploinsufficiency of GATA-2 perturbs adult hematopoietic stem-cell homeostasis. *Blood.* 2005;106(2):477-84.
55. Osellame LD, Blacker TS, and Duchen MR. Cellular and molecular mechanisms of mitochondrial function. *Best Pract Res Clin Endocrinol Metab.* 2012;26(6):711-23.
56. Hinge A, He J, Bartram J, Javier J, Xu J, Fjellman E, et al. Asymmetrically Segregated Mitochondria Provide Cellular Memory of Hematopoietic Stem Cell Replicative History and Drive HSC Attrition. *Cell Stem Cell.* 2020;26(3):420-30.e6.
57. Filippi MD, and Ghaffari S. Mitochondria in the maintenance of hematopoietic stem cells: new perspectives and opportunities. *Blood.* 2019;133(18):1943-52.
58. Cai X, Gao L, Teng L, Ge J, Oo ZM, Kumar AR, et al. Runx1 Deficiency Decreases Ribosome Biogenesis and Confers Stress Resistance to Hematopoietic Stem and Progenitor Cells. *Cell Stem Cell.* 2015;17(2):165-77.
59. Corces MR, Chang HY, and Majeti R. Preleukemic Hematopoietic Stem Cells in Human Acute Myeloid Leukemia. *Front Oncol.* 2017;7:263.
60. Reikvam H, Hatfield KJ, Kittang AO, Hovland R, and Bruserud Ø. Acute myeloid leukemia with the t(8;21) translocation: clinical consequences and biological implications. *J Biomed Biotechnol.* 2011;2011:104631.
61. Winters AC, and Bernt KM. MLL-Rearranged Leukemias-An Update on Science and Clinical Approaches. *Front Pediatr.* 2017;5:4.
62. Lawrence HJ, Rozenfeld S, Cruz C, Matsukuma K, Kwong A, Kömüves L, et al. Frequent co-expression of the HOXA9 and MEIS1 homeobox genes in human myeloid leukemias. *Leukemia.* 1999;13(12):1993-9.

63. Dorsam ST, Ferrell CM, Dorsam GP, Derynck MK, Vijapurkar U, Khodabakhsh D, et al. The transcriptome of the leukemogenic homeoprotein HOXA9 in human hematopoietic cells. *Blood.* 2004;103(5):1676-84.
64. Somervaille TC, and Cleary ML. Identification and characterization of leukemia stem cells in murine MLL-AF9 acute myeloid leukemia. *Cancer Cell.* 2006;10(4):257-68.
65. Bonnet D, and Dick JE. Human acute myeloid leukemia is organized as a hierarchy that originates from a primitive hematopoietic cell. *Nat Med.* 1997;3(7):730-7.
66. Menendez-Gonzalez JB, Vukovic M, Abdelfattah A, Saleh L, Almotiri A, Thomas LA, et al. Gata2 as a Crucial Regulator of Stem Cells in Adult Hematopoiesis and Acute Myeloid Leukemia. *Stem Cell Reports.* 2019;13(2):291-306.
67. Gregoire JM, and Romeo PH. T-cell expression of the human GATA-3 gene is regulated by a non-lineage-specific silencer. *J Biol Chem.* 1999;274(10):6567-78.
68. Hosoya T, Kuroha T, Moriguchi T, Cummings D, Maillard I, Lim KC, et al. GATA-3 is required for early T lineage progenitor development. *J Exp Med.* 2009;206(13):2987-3000.
69. Guan T, Dominguez CX, Amezquita RA, Laidlaw BJ, Cheng J, Henao-Mejia J, et al. ZEB1, ZEB2, and the miR-200 family form a counterregulatory network to regulate CD8(+) T cell fates. *J Exp Med.* 2018;215(4):1153-68.
70. Jansen CS, Prokhnevska N, Master VA, Sanda MG, Carlisle JW, Bilen MA, et al. An intra-tumoral niche maintains and differentiates stem-like CD8 T cells. *Nature.* 2019.
71. Boyd AS, and Rodrigues NP. Stem Cells Cycle toward Immune Surveillance. *Immunity.* 2018;48(2):187-90.
72. Noman MZ, Van Moer K, Marani V, Gemmill RM, Tranchevent LC, Azuaje F, et al. CD47 is a direct target of SNAI1 and ZEB1 and its blockade activates the phagocytosis of breast cancer cells undergoing EMT. *Oncoimmunology.* 2018;7(4):e1345415.
73. Teitell MA, and Mikkola HK. Transcriptional activators, repressors, and epigenetic modifiers controlling hematopoietic stem cell development. *Pediatr Res.* 2006;59(4 Pt 2):33R-9R.
74. Hock H, Hamblen MJ, Rooke HM, Schindler JW, Saleque S, Fujiwara Y, et al. Gfi-1 restricts proliferation and preserves functional integrity of haematopoietic stem cells. *Nature.* 2004;431(7011):1002-7.
75. Zeng H, Yucel R, Kosan C, Klein-Hitpass L, and Moroy T. Transcription factor Gfi1 regulates self-renewal and engraftment of hematopoietic stem cells. *The EMBO journal.* 2004;23(20):4116-25.
76. Florian MC, Klose M, Sacma M, Jablanovic J, Knudson L, Nattamai KJ, et al. Aging alters the epigenetic asymmetry of HSC division. *PLoS Biol.* 2018;16(9):e2003389.
77. Voog J, D'Alterio C, and Jones DL. Multipotent somatic stem cells contribute to the stem cell niche in the Drosophila testis. *Nature.* 2008;454(7208):1132-6.

78. Boyle M, Wong C, Rocha M, and Jones DL. Decline in self-renewal factors contributes to aging of the stem cell niche in the Drosophila testis. *Cell Stem Cell.* 2007;1(4):470-8.
79. Wu M, Kwon HY, Rattis F, Blum J, Zhao C, Ashkenazi R, et al. Imaging hematopoietic precursor division in real time. *Cell Stem Cell.* 2007;1(5):541-54.
80. Cayouette M, and Raff M. Asymmetric segregation of Numb: a mechanism for neural specification from Drosophila to mammals. *Nat Neurosci.* 2002;5(12):1265-9.
81. Jiang X, An W, Yang X, Lin J, Ma S, Wang D, et al. Asymmetric distribution of CRUMBS polarity complex proteins from compacted 8-cell to blastocyst stage during mouse preimplantation development. *Gene Expr Patterns.* 2018;27:93-8.
82. Roignot J, Peng X, and Mostov K. Polarity in mammalian epithelial morphogenesis. *Cold Spring Harb Perspect Biol.* 2013;5(2).
83. Takubo K, Nagamatsu G, Kobayashi CI, Nakamura-Ishizu A, Kobayashi H, Ikeda E, et al. Regulation of glycolysis by Pdk functions as a metabolic checkpoint for cell cycle quiescence in hematopoietic stem cells. *Cell Stem Cell.* 2013;12(1):49-61.
84. Yu WM, Liu X, Shen J, Jovanovic O, Pohl EE, Gerson SL, et al. Metabolic regulation by the mitochondrial phosphatase PTPMT1 is required for hematopoietic stem cell differentiation. *Cell Stem Cell.* 2013;12(1):62-74.
85. Donati G, Bertoni S, Brighenti E, Vici M, Treré D, Volarevic S, et al. The balance between rRNA and ribosomal protein synthesis up- and downregulates the tumour suppressor p53 in mammalian cells. *Oncogene.* 2011;30(29):3274-88.
86. Schreck C, Istvanffy R, Ziegenhain C, Sippenauer T, Ruf F, Henkel L, et al. Niche WNT5A regulates the actin cytoskeleton during regeneration of hematopoietic stem cells. *J Exp Med.* 2017;214(1):165-81.
87. Halaoui R, and McCaffrey L. Rewiring cell polarity signaling in cancer. *Oncogene.* 2015;34(8):939-50.
88. Vermeer MH, van Doorn R, Dijkman R, Mao X, Whittaker S, van Voorst Vader PC, et al. Novel and highly recurrent chromosomal alterations in Sezary syndrome. *Cancer Res.* 2008;68(8):2689-98.
89. Hidaka T, Nakahata S, Hatakeyama K, Hamasaki M, Yamashita K, Kohno T, et al. Down-regulation of TCF8 is involved in the leukemogenesis of adult T-cell leukemia/lymphoma. *Blood.* 2008;112(2):383-93.
90. Nakahata S, Yamazaki S, Nakauchi H, and Morishita K. Downregulation of ZEB1 and overexpression of Smad7 contribute to resistance to TGF-beta1-mediated growth suppression in adult T-cell leukemia/lymphoma. *Oncogene.* 2010;29(29):4157-69.
91. Sanchez-Tillo E, Fanlo L, Siles L, Montes-Moreno S, Moros A, Chiva-Blanch G, et al. The EMT activator ZEB1 promotes tumor growth and determines differential response to chemotherapy in mantle cell lymphoma. *Cell Death Differ.* 2014;21(2):247-57.
92. Stavropoulou V, Kaspar S, Brault L, Sanders MA, Juge S, Morettini S, et al. MLL-AF9 Expression in Hematopoietic Stem Cells Drives a Highly Invasive AML Expressing EMT-Related Genes Linked to Poor Outcome. *Cancer Cell.* 2016;30(1):43-58.

93. Basheer F, Giotopoulos G, Meduri E, Yun H, Mazan M, Sasca D, et al. Contrasting requirements during disease evolution identify EZH2 as a therapeutic target in AML. *J Exp Med.* 2019;216(4):966-81.
94. Liberzon A, Subramanian A, Pinchback R, Thorvaldsdottir H, Tamayo P, and Mesirov JP. Molecular signatures database (MSigDB) 3.0. *Bioinformatics.* 2011;27(12):1739-40.
95. Edgar R, Domrachev M, and Lash AE. Gene Expression Omnibus: NCBI gene expression and hybridization array data repository. *Nucleic Acids Res.* 2002;30(1):207-10.
96. Kolesnikov N, Hastings E, Keays M, Melnichuk O, Tang YA, Williams E, et al. ArrayExpress update--simplifying data submissions. *Nucleic Acids Res.* 2015;43(Database issue):D1113-6.
97. Menendez-Gonzalez JB, Sinnadurai S, Gibbs A, Thomas LA, Konstantinou M, Garcia-Valverde A, et al. Inhibition of GATA2 restrains cell proliferation and enhances apoptosis and chemotherapy mediated apoptosis in human GATA2 overexpressing AML cells. *Sci Rep.* 2019;9(1):12212.

Figure 1

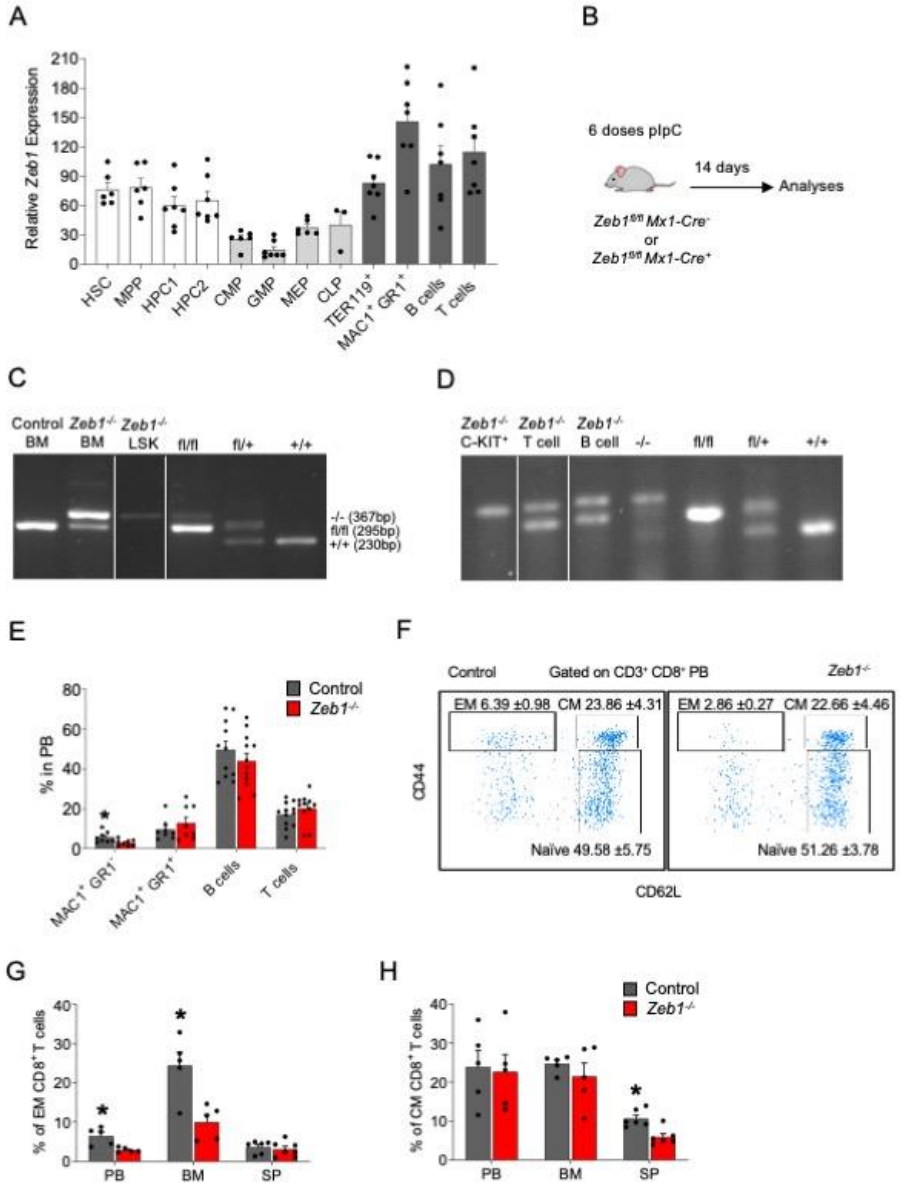
A
Relative Zeb1 Expression
HSC
MPP
HPC1
HPC2
CMP
GMP
MEP
CLP
TER119+
MAC1+ GR1+
B cells
T cells
B
6 doses pIpC
14 days
Analyses
Zeb1fl/fl Mx1-Cre-
or
Zeb1fl/fl Mx1-Cre+
C
Control BM
Zeb1-/- BM
Zeb1-/- LSK
fl/fl
fl/+
+/+
-/- (367bp)
fl/fl (295bp)
+/+ (230bp)
D
Zeb1-/- C-KIT+
Zeb1-/- T cell
Zeb1-/- B cell
-/-
fl/fl
fl/+
+/+
E
% in PB
Control
Zeb1-/-
MAC1+ GR1-
MAC1+ GR1+
B cells
T cells
F
Control
Gated on CD3+ CD8+ PB
Zeb1-/-
EM 6.39 ±0.98
CM 23.86 ±4.31
EM 2.86 ±0.27
CM 22.66 ±4.46
Naïve 49.58 ±5.75
Naïve 51.26 ±3.78
CD44
CD62L
G
% of EM CD8+ T cells
PB
BM
SP
H
Control
Zeb1-/-
% of CM CD8+ T cells
PB
BM
SP

Figure 1. Loss of *Zeb1* impacts effector and central memory CD8$^+$ T cells. (A) RT Q-PCR analysis of mRNA *Zeb1* expression in different hematopoietic populations (n=6-7 except CLP n=3). (B) A scheme of pIpC treatment to delete *Zeb1* in *Zeb1$^{fl/fl}$ Mx1-Cre$^-$* (control) and *Zeb1$^{fl/fl}$ Mx1- Cre$^+$* (*Zeb1$^{-/-}$*) mice and analysis at D14 after the last pIpC dose. (C) Representative gel electrophoresis analysis confirming *Zeb1* deletion in BM cells and LSK population 14 days after the last dose of pIpC. (D) Representative gel electrophoresis analysis of *Zeb1* deletion in BM C-KIT$^+$ cells, spleen B (B220$^+$) and T (CD3$^+$) cells 14 days after the last dose of pIpC. (E) The frequency of differentiated cells in PB from control and *Zeb1$^{-/-}$* mice 14 days after the last dose of pIpC from 4 independent experiments (n= 8-12 per group). (F) The gating strategy of naïve, effector memory (EM) and central memory (CM) T cells using CD62L and CD44 markers along with T cell markers CD3, CD4, and CD8 in PB. The frequency of EM T cells (G) and CM T cells (H) within CD3$^+$ CD8$^+$ T cells in PB, BM, and SP from control (n= 5 PB and BM, 6 SP) and *Zeb1$^{-/-}$* (n= 5 PB and BM, 6-7 SP) mice from 2 independent experiments. Error bars show mean ± SEM. Mann-Whitney U test was used to calculate significance as follows: *P < .05, **P < .01, ***P < .001, ****P <0.0001.

Figure 2

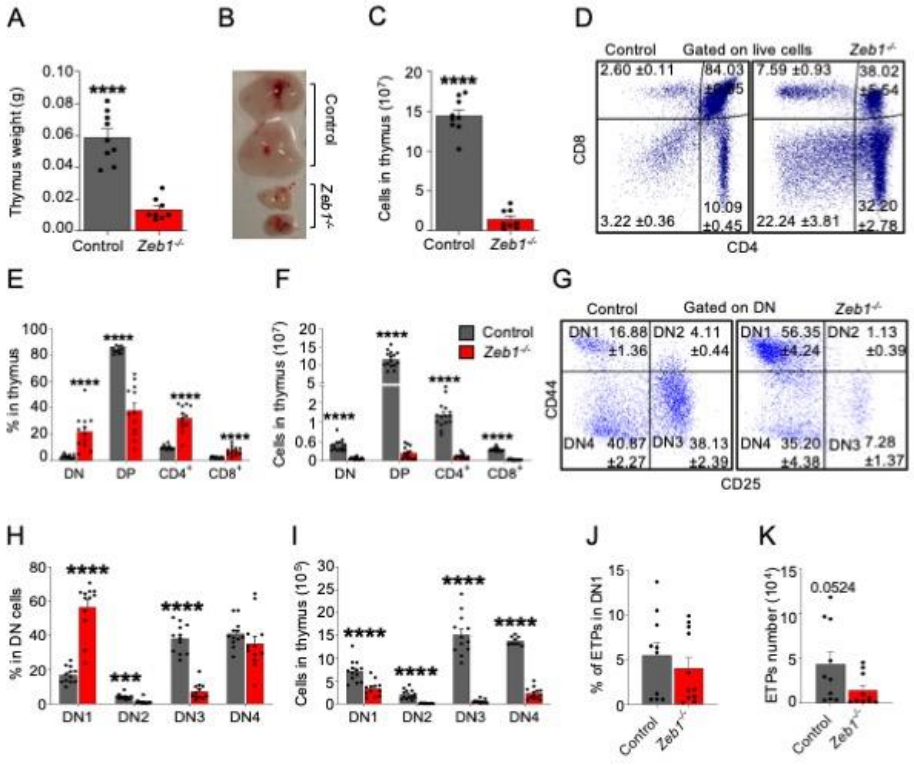
A
B
C
D
Thymus weight (g)
Control
Zeb1-/-
Cells in thymus (10^7)
Gated on live cells
CD8
CD4
2.60 ±0.11
84.03 ±0.95
7.59 ±0.93
38.02 ±5.54
3.22 ±0.36
10.09 ±0.45
22.24 ±3.81
32.20 ±2.78
E
F
G
% in thymus
DN
DP
CD4+
CD8+
Gated on DN
CD44
CD25
DN1 16.88 ±1.36
DN2 4.11 ±0.44
DN1 56.35 ±4.24
DN2 1.13 ±0.39
DN4 40.87 ±2.27
DN3 38.13 ±2.39
DN4 35.20 ±4.38
DN3 7.28 ±1.37
H
I
J
K
% in DN cells
DN1
DN2
DN3
DN4
% of ETPs in DN1
ETPs number (10^4)
0.0524

Figure 2. Loss of *Zeb1* results in T cell reduction in thymus associated with early differentiation defects in thymus. Thymus weight (A), a representative picture (B) and total thymus cellularity (C) from control (n=9) and *Zeb1*$^{-/-}$ (n=8) mice from 5 independent experiments at D14 after the last pIpC dose. (D) Representative FACS plots of T cell analysis in thymus based on CD4 and CD8 cell surface markers (DN: CD4^{-} CD8^{-} , DP: CD4^{+} CD8^{+}, CD4^{+}, CD8^{+}). (E) Frequency of T cell subsets in thymus from control (n=13) and *Zeb1*$^{-/-}$ (n=12) mice from 6 independent experiments at D14 after the last pIpC dose. (F) Total cell count of T cell subsets in thymus from control (n=14-15) and *Zeb1*$^{-/-}$ (n=14-15) mice from 7 independent experiments at D14 after the last pIpC dose. (G) Representative FACS plots showing the gating strategy of early stages within CD4 CD8 DN population using CD25 and CD44 (DN1: CD44^{+} CD25^{-}, DN2: CD44^{+} CD25^{+}, DN3: CD44^{-} CD25^{+}, DN4: CD44^{-} CD25^{-}) between control and *Zeb1*$^{-/-}$ at D14 after the last pIpC dose. (H) Frequency of DN populations (DN1, DN2, DN3, DN4) in DN cells from control (n=12) and *Zeb1*$^{-/-}$ (n=12) mice from 5 independent experiments at D14 after the last pIpC dose. (I) Total cell count of DN populations in thymus from control (n=9-13) and *Zeb1*$^{-/-}$ (n=11-13) mice from 4 independent experiments at D14 after the last pIpC dose. (J) The frequency and (K) the total count of ETPs (DN1 cKit^{high}) from control (n=10) and *Zeb1*$^{-/-}$ (n=10-11) mice from 4 independent experiments at D14 after the last pIpC dose. Error bars show mean ± SEM. Mann-Whitney U test was used to calculate significance as follows: *P < .05, **P < .01, ***P < .001, ****P <0.0001.

Figure 3

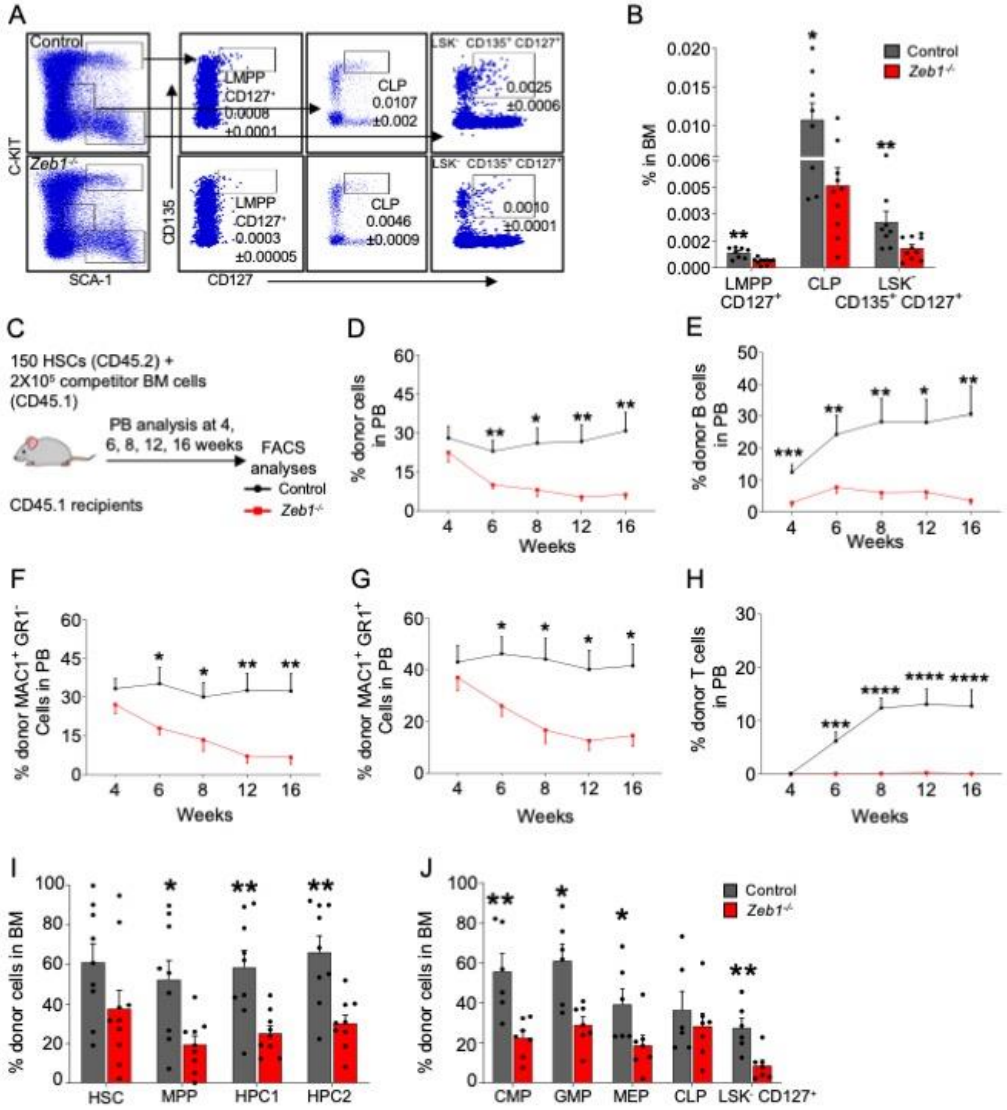
A
Control
Zeb1-/-
C-KIT
SCA-1
CD135
CD127
LMPP CD127+ 0.0008 ±0.0001
CLP 0.0107 ±0.002
LSK- CD135+ CD127+ 0.0025 ±0.0006
LMPP CD127+ 0.0003 ±0.00005
CLP 0.0046 ±0.0009
LSK- CD135+ CD127+ 0.0010 ±0.0001
B
% in BM
Control
Zeb1-/-
LMPP CD127+
CLP
LSK- CD135+ CD127+
C
150 HSCs (CD45.2) +
2X10^5 competitor BM cells
(CD45.1)
PB analysis at 4, 6, 8, 12, 16 weeks
FACS analyses
CD45.1 recipients
Control
Zeb1-/-
D
% donor cells in PB
Weeks
E
% donor B cells in PB
Weeks
F
% donor MAC1+ GR1- Cells in PB
Weeks
G
% donor MAC1+ GR1+ Cells in PB
Weeks
H
% donor T cells in PB
Weeks
I
% donor cells in BM
HSC
MPP
HPC1
HPC2
J
% donor cells in BM
Control
Zeb1-/-
CMP
GMP
MEP
CLP
LSK- CD127+

Figure 3. Loss of *Zeb1* results in a reduction of lymphoid progenitors in BM and a multilineage hematopoietic differentiation defect after HSC transplantation. (A) Representative FACS plots of the analysis of LMPP $CD127^+$ (non-conventional LMPP: LSK $CD135^+$ $CD127^+$), CLP (LIN^- $SCA\text{-}1^{low}$ $C\text{-}KIT^{low}$ $CD135^+$ $CD127^+$), and LSK^- $CD127^+$ $CD135^+$ 14 days after the last dose of pIpC. (B) Frequency of LMPP $CD127^+$, CLP, and LSK^- $CD127^+$ $CD135^+$ in the BM from control (n=8) and *Zeb1*$^{-/-}$ (n=10) mice from 4 independent experiments at D14 after the last pIpC dose. (C) A scheme of the competitive HSC transplantation. 150 HSCs from control or *Zeb1*$^{-/-}$ mice (donor CD45.2) mixed with $2X10^5$ BM competitor cells (CD45.1) were transplanted into lethally irradiated recipients (CD45.1) and the mice were monitored by bleeding the tail vein at different time points until week 16. (D) The percentage of donor cells in PB at different time points post HSC transplantation from control (n=10) and *Zeb1*$^{-/-}$ (n= 10) mice from 3 independent experiments. Analysis of PB donor contribution to B cells ($B220^+$) (E), $MAC1^+$ $GR1^-$ myeloid cells (F), $MAC1^+$ $GR1^+$ myeloid cells (G), and T cells ($CD4^+$ $CD8^+$) (H) from control (n=10) and *Zeb1*$^{-/-}$ (n=8-10) mice from 3 independent experiments. Donor contribution to BM HSPCs (I) (HSC: LSK $CD150^+$ $CD48^-$, MPP: LSK $CD150^-$ $CD48^-$, HPC1: LSK $CD150^-$ $CD48^+$, HPC2: LSK $CD150^+$ $CD48^+$) from control (n=9) and *Zeb1*$^{-/-}$ (n=9) from 3 independent experiments and BM committed progenitors (J) (CMP: LK $CD34^+$ $CD16/32^-$, GMP: $CD34^+$ $CD16/32^+$, MEP: $CD34^-$ $CD16/32^-$, CLP: LIN^- $SCA\text{-}1^{low}$ $C\text{-}KIT^{low}$ $CD127^+$, and LSK^- $CD127^+$ from control (n=6) and *Zeb1*$^{-/-}$ (n=7) from 2 independent experiments. Error bars show mean ± SEM. Mann-Whitney U test was used to calculate significance as follows: *P < .05, **P < .01, ***P < .001, ****P <0.0001.

Figure 4

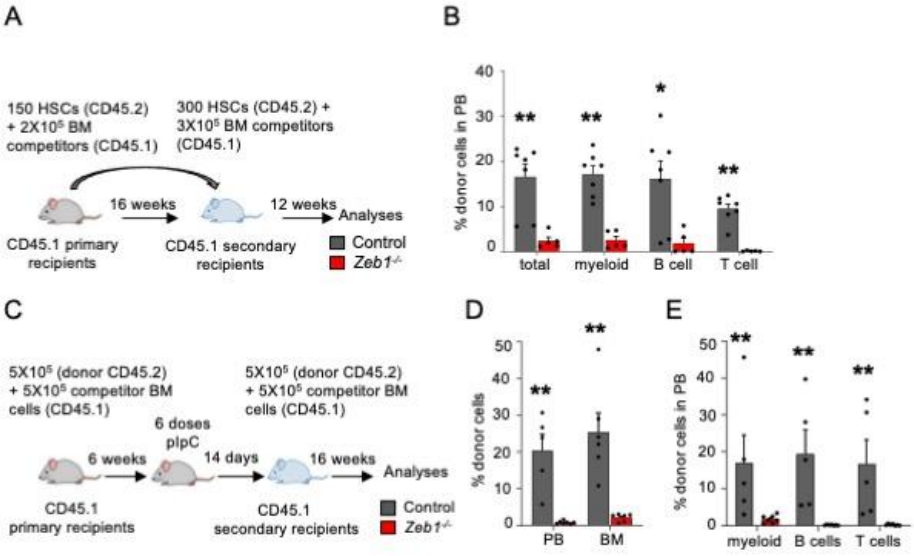
A
150 HSCs (CD45.2)
+ 2X10⁵ BM
competitors (CD45.1)
300 HSCs (CD45.2) +
3X10⁵ BM competitors
(CD45.1)
16 weeks
12 weeks
Analyses
CD45.1 primary
recipients
CD45.1 secondary
recipients
Control
Zeb1-/-
B
% donor cells in PB
total
myeloid
B cell
T cell
C
5X10⁵ (donor CD45.2)
+ 5X10⁵ competitor BM
cells (CD45.1)
5X10⁵ (donor CD45.2)
+ 5X10⁵ competitor BM
cells (CD45.1)
6 doses
pIpC
6 weeks
14 days
16 weeks
Analyses
CD45.1
primary recipients
CD45.1
secondary recipients
Control
Zeb1-/-
D
% donor cells
PB
BM
E
% donor cells in PB
myeloid
B cells
T cells

Figure 4. *Zeb1* regulates HSC self-renewal and differentiation in a cell autonomous manner. (A) Schema of the secondary HSC transplantation. 300 CD45.2^{+} HSCs from primary recipients from control or *Zeb1*$^{-/-}$ mice mixed with 3X10^{5} BM competitor cells (CD45.1) were transplanted into lethally irradiated recipients (CD45.1) and the mice were analysed at week 12. (B) The percentage of donor cells in PB and donor contribution to myeloid (MAC1^{+}), B (B220^{+}), and T (CD4^{+}/CD8^{+}) cells at week 12 post-secondary HSC transplantation from control (n=7) and *Zeb1*$^{-/-}$ (n=5) from 2 independent experiments. (C) Schema of the secondary total BM transplantation in cell autonomous manner. 5X10^{5} CD45.2^{+} BM cells from primary recipients 14 days after the last pIpC dose from control or *Zeb1*$^{-/-}$ mice mixed with 5X10^{5} BM competitor cells (CD45.1) were transplanted into lethally irradiated recipients (CD45.1) and the mice were analysed at week 16. (D) The percentage of donor cells in PB and BM at week 16 post-secondary cell autonomous total BM transplantation from control (PB n=5, BM=6) and *Zeb1*$^{-/-}$ (PB n= 7, BM=6) mice from one experiment. (E) Donor contribution to PB MAC1^{+} myeloid cells, B220^{+} B cells, and CD4^{+}/CD8^{+} T cells at week 16 post-secondary cell autonomous total BM transplantation from control (n=5) and *Zeb1*$^{-/-}$ (n=7) mice from one experiment. Error bars show mean ± SEM. Mann-Whitney U test was used to calculate significance as follows: *P < .05, **P < .01, ***P < .001, ****P <0.0001.

Figure 5

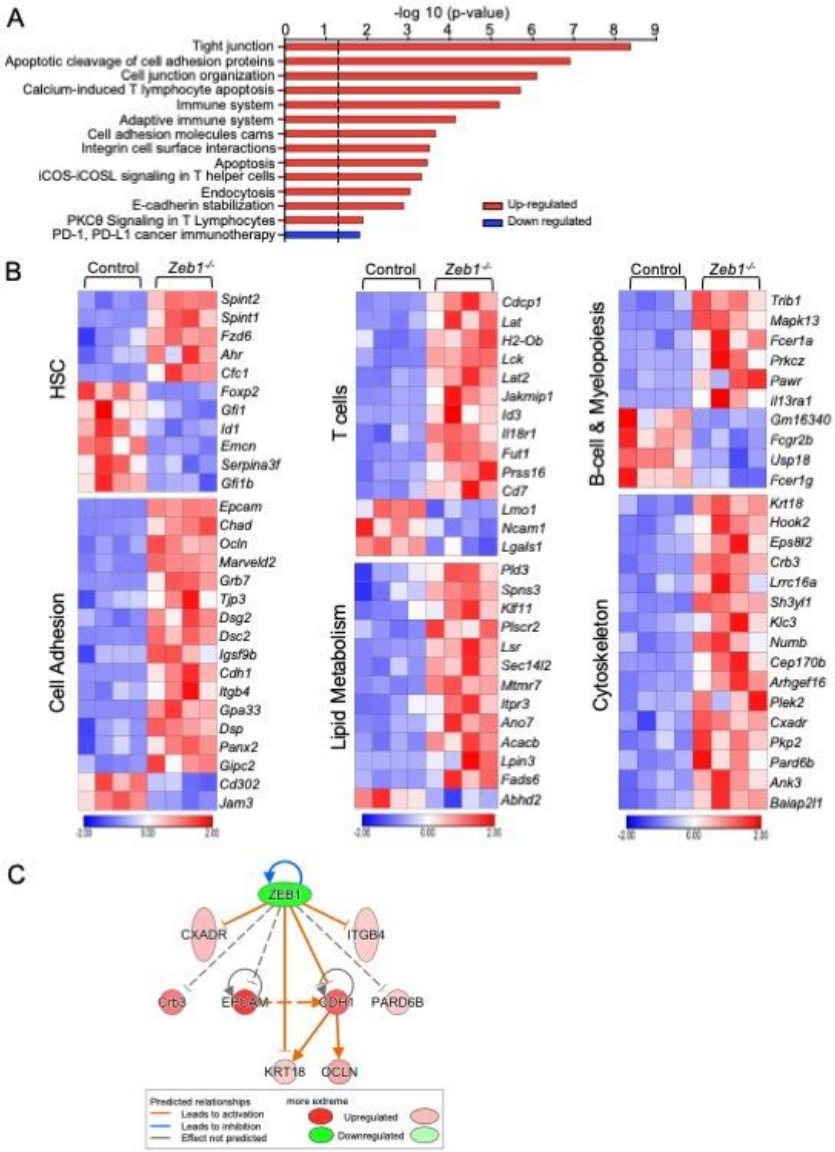
A
-log 10 (p-value)
0 1 2 3 4 5 6 7 8 9
Tight junction
Apoptotic cleavage of cell adhesion proteins
Cell junction organization
Calcium-induced T lymphocyte apoptosis
Immune system
Adaptive immune system
Cell adhesion molecules cams
Integrin cell surface interactions
Apoptosis
iCOS-iCOSL signaling in T helper cells
Endocytosis
E-cadherin stabilization
PKCθ Signaling in T Lymphocytes
PD-1, PD-L1 cancer immunotherapy
Up-regulated
Down regulated
B
Control
Zeb1-/-
HSC
Spint2
Spint1
Fzd6
Ahr
Cfc1
Foxp2
Gfi1
Id1
Emcn
Serpina3f
Gfi1b
Cell Adhesion
Epcam
Chad
Ocln
Marveld2
Grb7
Tjp3
Dsg2
Dsc2
Igsf9b
Cdh1
Itgb4
Gpa33
Dsp
Panx2
Gipc2
Cd302
Jam3
T cells
Cdcp1
Lat
H2-Ob
Lck
Lat2
Jakmip1
Id3
Il18r1
Fut1
Prss16
Cd7
Lmo1
Ncam1
Lgals1
Lipid Metabolism
Pld3
Spns3
Klf11
Plscr2
Lsr
Sec14l2
Mtmr7
Itpr3
Ano7
Acacb
Lpin3
Fads6
Abhd2
B-cell & Myelopoiesis
Trib1
Mapk13
Fcer1a
Prkcz
Pawr
Il13ra1
Gm16340
Fcgr2b
Usp18
Fcer1g
Cytoskeleton
Krt18
Hook2
Eps8l2
Crb3
Lrrc16a
Sh3yl1
Klc3
Numb
Cep170b
Arhgef16
Plek2
Cxadr
Pkp2
Pard6b
Ank3
Baiap2l1
C
ZEB1
CXADR
ITGB4
Crb3
EPCAM
CDH1
PARD6B
KRT18
OCLN
Predicted relationships
Leads to activation
Leads to inhibition
Effect not predicted
more extreme
Upregulated
Downregulated

Figure 5. *Zeb1*$^{-/-}$ HSCs display deregulation of hematopoietic function and cell polarity transcriptional programming. RNA sequencing was performed in sorted control and *Zeb1*$^{-/-}$ HSCs (LSK CD150^{+} CD48^{-}) 14 days after the last pIpC dose (n=4 for each genotype). (A) Biological pathway analysis shows the top enriched pathways in *Zeb1*$^{-/-}$ HSCs compared to control. Data is shown as –log10 (p-value), and the dashed black line indicates p-value = 0.05. (B) Heat maps of the differentially expressed genes after *Zeb1* deletion related to HSC function, T cells and B cells as well as cytoskeleton, lipid metabolism, and cell adhesion. The heatmap scale represents Z-score. (C) A network of *Zeb1* interaction with several target genes related to polarity, cytoskeleton, and cell adhesion using Ingenuity Pathway Analysis (IPA) software. Due to their confirmed binding to ZEB1 in the literature, Epcam, Pard6b, and Crb3 were added manually.

Figure 6

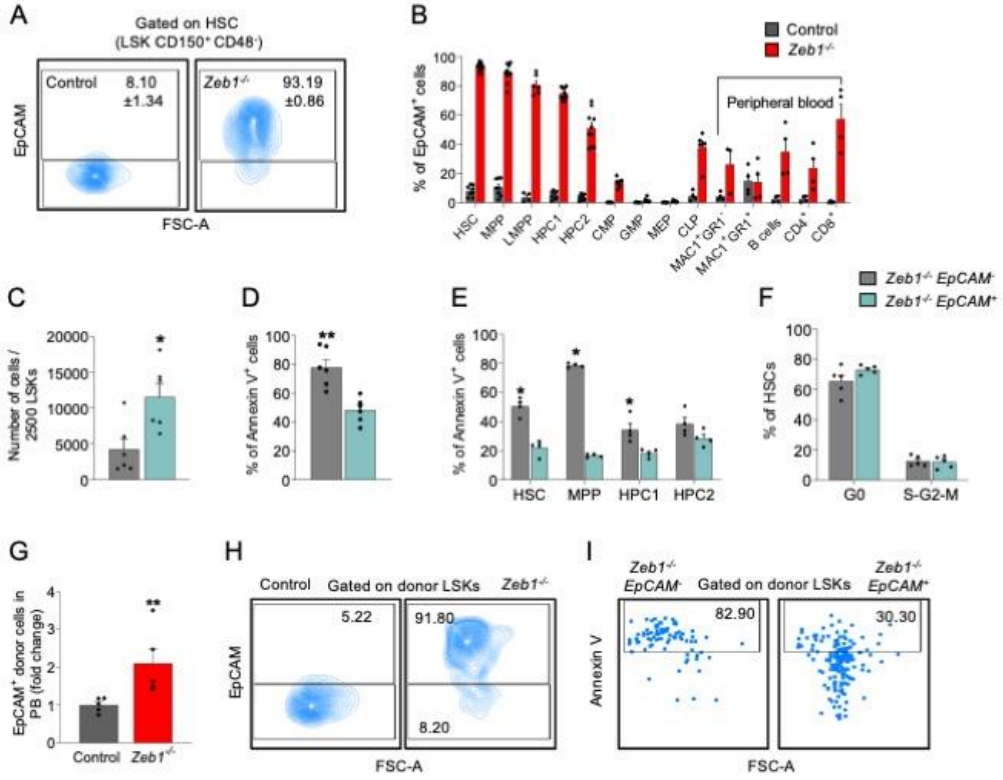
A
Gated on HSC
(LSK CD150+ CD48-)
Control
8.10
±1.34
Zeb1-/-
93.19
±0.86
EpCAM
FSC-A
B
Control
Zeb1-/-
% of EpCAM+ cells
Peripheral blood
HSC
MPP
LMPP
HPC1
HPC2
CMP
GMP
MEP
CLP
MAC1+GR1-
MAC1+GR1+
B cells
CD4+
CD8+
C
Number of cells / 2500 LSKs
D
% of Annexin V+ cells
E
% of Annexin V+ cells
HSC
MPP
HPC1
HPC2
F
Zeb1-/- EpCAM-
Zeb1-/- EpCAM+
% of HSCs
G0
S-G2-M
G
EpCAM+ donor cells in PB (fold change)
Control
Zeb1-/-
H
Control
Gated on donor LSKs
Zeb1-/-
5.22
91.80
8.20
EpCAM
FSC-A
I
Zeb1-/- EpCAM-
Gated on donor LSKs
Zeb1-/- EpCAM+
82.90
30.30
Annexin V
FSC-A

Figure 6. Increased EpCAM expression confers survival advantage and differentiation block in *Zeb1*$^{-/-}$ HSCs. (A) Representative flow cytometry plots of EpCAM expression in HSCs 14 days after pIpC injection. (B) Analysis of EpCAM expression in BM subpopulations and PB mature cells 14 days after pIpC injection from control (n=8 for HSC, MPP, HPC1, and HPC2; n=4 for LMPP, CLP and mature PB populations; n=5 for CMP, GMP, and MEP) and *Zeb1*$^{-/-}$ (n=10 for HSC, MPP, HPC1, and HPC2; n=6 for LMPP and CLP; n= 4 for mature PB populations except MAC1^{+} GR1^{-} n=3; n=7 for CMP, GMP, and MEP). (C) Cell number after culturing 2500 LSKs from *Zeb1*$^{-/-}$ *EpCAM*$^{-}$ (n=6) and *Zeb1*$^{-/-}$ *EpCAM*$^{+}$ (n=6) from 3 independent experiments. (D) Analysis of apoptosis in LSKs post culture from *Zeb1*$^{-/-}$ *EpCAM*$^{-}$ (n=6) and *Zeb1*$^{-/-}$ *EpCAM*$^{+}$ (n=6) from 3 independent experiments. (E) Analysis of apoptosis in fresh BM HSPCs 14 days after pIpC injection from *Zeb1*$^{-/-}$ *EpCAM*$^{-}$ (n=4) and *Zeb1*$^{-/-}$ *EpCAM*$^{+}$ (n=4) from 2 independent experiments. (F) Cell cycle analysis of HSCs using Ki67 and DAPI 14 days after pIpC injection from *Zeb1*$^{-/-}$ *EpCAM*$^{-}$ (n=5) and *Zeb1*$^{-/-}$ *EpCAM*$^{+}$ (n=5) from one experiment. (G) Analysis of EpCAM expression in donor PB at week 16 after primary HSC transplantation from control (n=5) and *Zeb1*$^{-/-}$ (n=5) from one experiment represented as fold change. (H) Representative FACS plots of the analysis of EpCAM expression in LSKs 16 weeks post primary HSC transplantation from control (n=2) and *Zeb1*$^{-/-}$ (n=1) from one experiment. (I) Representative FACS plots of the analysis of apoptosis using Annexin V in EpCAM negative and positive fractions within donor LSKs 16 weeks post primary HSC transplantation from control (n=2) and *Zeb1*$^{-/-}$ (n=1) from one experiment. Error bars show mean ± SEM. Mann-Whitney U test was used to calculate significance as follows: *P < .05, **P < .01, ***P < .001, ****P <0.0001.

Figure 7

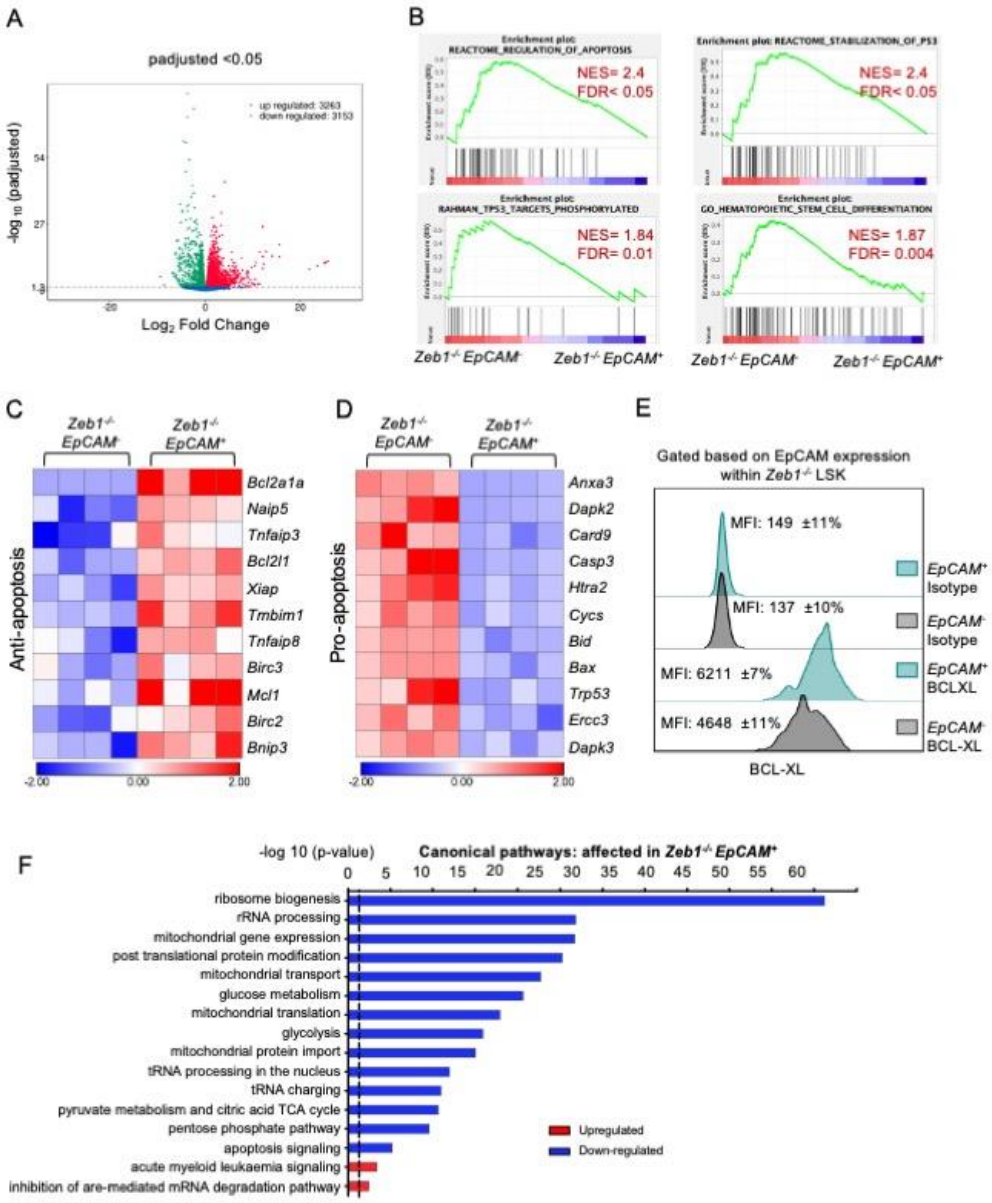
A
padjusted <0.05
up regulated: 3263
down regulated: 3153
-log 10 (padjusted)
Log2 Fold Change
B
Enrichment plot: REACTOME_REGULATION_OF_APOPTOSIS
NES= 2.4
FDR< 0.05
Enrichment plot: REACTOME_STABILIZATION_OF_P53
NES= 2.4
FDR< 0.05
Enrichment plot: RAHMAN_TP53_TARGETS_PHOSPHORYLATED
NES= 1.84
FDR= 0.01
Enrichment plot: GO_HEMATOPOIETIC_STEM_CELL_DIFFERENTIATION
NES= 1.87
FDR= 0.004
Zeb1-/- EpCAM- Zeb1-/- EpCAM+
Zeb1-/- EpCAM- Zeb1-/- EpCAM+
C
Zeb1-/- EpCAM-
Zeb1-/- EpCAM+
Anti-apoptosis
Bcl2a1a
Naip5
Tnfaip3
Bcl2l1
Xiap
Tmbim1
Tnfaip8
Birc3
Mcl1
Birc2
Bnip3
-2.00
0.00
2.00
D
Zeb1-/- EpCAM-
Zeb1-/- EpCAM+
Pro-apoptosis
Anxa3
Dapk2
Card9
Casp3
Htra2
Cycs
Bid
Bax
Trp53
Ercc3
Dapk3
-2.00
0.00
2.00
E
Gated based on EpCAM expression within Zeb1-/- LSK
MFI: 149 ±11%
EpCAM+ Isotype
MFI: 137 ±10%
EpCAM- Isotype
MFI: 6211 ±7%
EpCAM+ BCLXL
MFI: 4648 ±11%
EpCAM- BCL-XL
BCL-XL
F
-log 10 (p-value)
Canonical pathways: affected in Zeb1-/- EpCAM+
0 5 10 15 20 25 30 35 40 45 50 55 60
ribosome biogenesis
rRNA processing
mitochondrial gene expression
post translational protein modification
mitochondrial transport
glucose metabolism
mitochondrial translation
glycolysis
mitochondrial protein import
tRNA processing in the nucleus
tRNA charging
pyruvate metabolism and citric acid TCA cycle
pentose phosphate pathway
apoptosis signaling
acute myeloid leukaemia signaling
inhibition of are-mediated mRNA degradation pathway
Upregulated
Down-regulated

Figure 7. *Zeb1*$^{-/-}$ *EpCAM*$^{+}$ HSPCs display enhanced cell survival and diminished mitochondrial metabolism, RNA biogenesis and differentiation transcriptional signatures. (A) a volcano plot showing the relationship between magnitude of gene expression change (log_2 of fold-change; x-axis) and statistical significance of this change [-log_{10} of adjusted p-value; y-axis] in a comparison of *Zeb1*$^{-/-}$ *EpCAM*$^{+}$ to *Zeb1*$^{-/-}$ *EpCAM*$^{-}$ LSK cells. Coloured points represent differentially expressed genes (cut-off FDR < 0.05) that are either overexpressed (red) or under expressed (green) in *Zeb1*$^{-/-}$ *EpCAM*$^{+}$ compared to *Zeb1*$^{-/-}$ *EpCAM*$^{-}$. (B) GSEA plots of regulation of apoptosis, stabilization of P53, TP53 targets phosphorylated and hematopoietic stem cell differentiation. Heat maps of the differentially expressed genes within *EpCAM*$^{+}$ and *EpCAM*$^{-}$ LSK after *Zeb1* deletion related to anti-apoptosis (C) and pro-apoptosis (D). (E) A representative histogram of BCL-XL levels in EpCAM fractions within *Zeb1*$^{-/-}$ LSK. (F) Canonical pathways that mostly enriched in *Zeb1*$^{-/-}$ *EpCAM*$^{+}$ LSK cells derived from the IPA, BioCarta, KEGG, PID and Reactome pathway databases. Data is shown as –log10 (p-value), and the dashed black line indicates p- value = 0.05, the analysis was performed using the GSEA software and IPA.

Figure 8

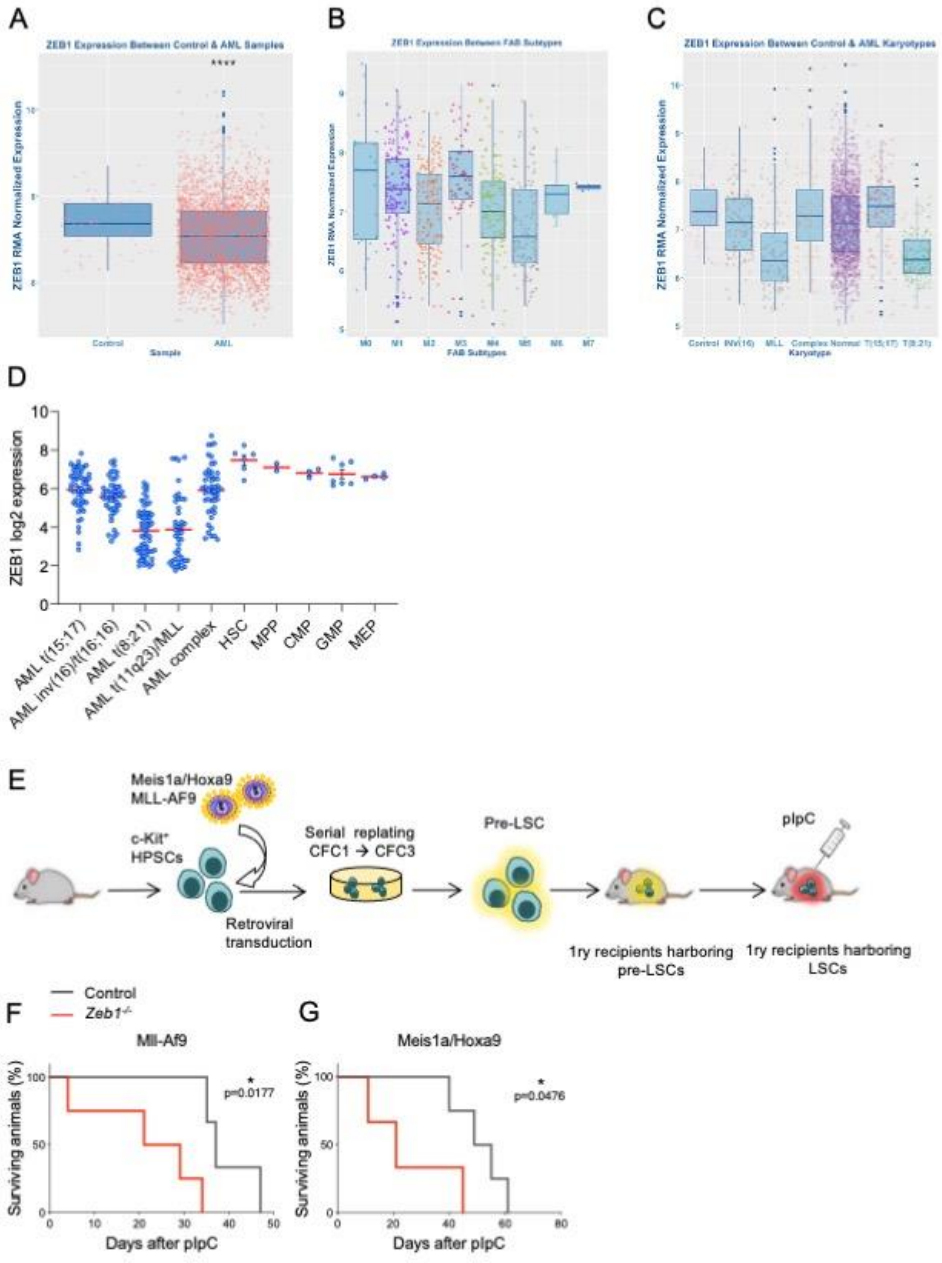
A
ZEB1 Expression Between Control & AML Samples
ZEB1 RMA Normalized Expression
Control
AML
Sample
B
ZEB1 Expression Between FAB Subtypes
ZEB1 RMA Normalized Expression
M0
M1
M2
M3
M4
M5
M6
M7
FAB Subtypes
C
ZEB1 Expression Between Control & AML Karyotypes
ZEB1 RMA Normalized Expression
Control
INV(16)
MLL
Complex
Normal
T(15;17)
T(8;21)
Karyotype
D
ZEB1 log2 expression
AML t(15;17)
AML inv(16)/t(16;16)
AML t(8;21)
AML t(11q23)/MLL
AML complex
HSC
MPP
CMP
GMP
MEP
E
Meis1a/Hoxa9
MLL-AF9
c-Kit+
HPSCs
Retroviral
transduction
Serial replating
CFC1 → CFC3
Pre-LSC
pIpC
1ry recipients harboring
pre-LSCs
1ry recipients harboring
LSCs
F
Control
Zeb1-/-
Mll-Af9
Surviving animals (%)
p=0.0177
Days after pIpC
G
Meis1a/Hoxa9
Surviving animals (%)
p=0.0476
Days after pIpC

Figure 8. *Zeb1* is downregulated in AML patient samples and acts as a tumour suppressor in MLL-AF9 and Meis1a/Hoxa9-driven AML. (A-C) ZEB1 RMA normalised expression from combined published datasets in (A) control and AML, (B) across FAB subtypes and, (C) karyotypes. (D) ZEB1 Log2 expression data in human HSPC and AML karyotypes. Data from Bloodspot (www.bloodspot.eu). Error bars show mean ± SEM. Student t-test was used unless otherwise indicated to calculate significance as follows: *P < .05, **P < .01, ***P < .001, ****P <0.0001. (E) C-KIT$^+$ cells from control and *Zeb1*$^{fl/fl}$ *Mx1-Cre*$^+$ mice were transduced with retroviruses expressing MLL-AF9 or Meis1a/Hoxa9 oncogenes and plated into colony-forming-cell (CFC) assays. After CFC3 (6 days each CFC), pre-LSCs (CD45.2$^+$ C-KIT$^+$) were sorted and transplanted into lethally-irradiated recipients together with CD45.1$^+$ unfractionated BM cells. Three weeks later, mice were administered pIpC to induce gene deletion and monitored for AML development. (F and G) Kaplan-Meier survival curve of primary recipients transplanted with (F) MLL-AF9 (n = 4) or (G) Meis1a/Hoxa9 (n = 4) preLSCs. Statistical analyses: Mantel-Cox test.